FUDMA Journal of Sciences (FJS)
ISSN online: 2616-1370
ISSN print: 2645 - 2944
Vol. 10 No. 7, April, 2026, pp 202 – 222
DOI: https://doi.org/10.33003/fjs-2026-1007-4973

MULTI-TARGET NEUROPROTECTIVE POTENTIAL OF CAMELLIA SINENSIS PHYTOCHEMICALS AGAINST PARKINSON'S DISEASE: AN INTEGRATED COMPUTATIONAL STUDY

[1,2]Abosede Adejoke Badeji

[1] Department of Chemical Sciences, Tai Solarin Federal University of Education, Ijagun, Ogun State, Nigeria.
[2] Centre of Molecular Medicine and Diagnostics (COMManD), Saveetha Dental College & Hospitals, Saveetha Institute of Medical and Technical Sciences, Saveetha University, Chennai, India.

*Corresponding authors' email: ogunlanaaa@tasued.edu.ng

ABSTRACT

Neurodegenerative diseases, especially Parkinson's disease (PD), have been a huge challenge to humanity, emphasizing the need for urgent attention towards finding more potent and less toxic treatment strategies. In this regard, this study employed a multi-faceted approach using density functional theory, molecular docking, molecular dynamics simulations, MM/PBSA free energy calculation, and in silico pharmacokinetic analysis to investigate the effectiveness of 25 phytochemicals extracted from *Camellia sinensis* on three PD-related targets: LRRK2, adenosine A2A receptor (A2AR), and monoamine oxidase-B (MAO-B). Docking analysis results revealed Petunidin, Cyanidin, and Epigallocatechin as potent compounds with high affinity for the targets. MD simulation results further corroborated this finding with stable ligand-target interactions. MM-PBSA results revealed Petunidin as the most potent multi-target compound with a high binding free energy of -38.48 kcal/mol for LRRK2 and -44.49 kcal/mol for MAO-B, surpassing the potency of reference compounds. Cyanidin ranked second. Among the compounds, Epigallocatechin showed the highest affinity for A2AR with a free energy of -36.43 kcal/mol. Stability analysis revealed a constant RMSD value for the compounds, indicating a stable complex. The pharmacokinetic profile revealed that the compounds complied with Lipinski's rule of five and showed high gastrointestinal absorption alongside and potential of CYP1A2 inhibition. DFT analysis revealed Malvidin and Petunidin with the lowest HOMO-LUMO gap of approximately 5.90 eV, indicating high reactivity. Cyanidin showed the highest electrophilicity index of 10.266 eV. NBO and MEP analysis revealed a high charge delocalization effect, with hydroxyl groups being electron-rich, facilitating hydrogen bonding and π-π interactions with the target proteins.

Keywords: *Camellia sinesis* phytochemicals, Density Functional Theory, Parkinson's disease, Molecular docking, Molecular dynamics, Pharmacokinetics, Drug-likeness

INTRODUCTION

The quest for effective treatments for neurodegenerative diseases frequently lead us back to natural products (Mohd Sairazi & Sirajudeen, 2020; Goyal *et al*., 2024). For centuries, natural products have played an important role as a source of medicines, including the remarkable diversity of complex molecules that have evolved to impart effects on biological systems (Li & Vederas, 2009). Today, the use of advanced technologies have helped researcher to finally understand how these natural products work on a molecular scale, especially for complex diseases like Parkinson's (Atanasov *et al*., 2021).

Parkinson's disease (PD), which is a neurodegenerative disorder, is a gradual loss of dopamine-producing neurons in the brain, arising from a storm of causes such as oxidative stress, mitochondrial dysfunction, and the harmful accumulation of α-synuclein fibrils, forming Lewy bodies in various brain regions (Koeglsperger *et al*., 2023; Saramowicz *et al*., 2023). The degeneration of this neurons results in motor symptoms including bradykinesia, rigidity, tremor and postural instability, as well as non-motor symptoms including sleep disturbances and cognitive decline (Saini *et al*., 2024; Rinaldi, 2025). The global occurrence of PD has been on the increase over recent decades, especially in high human development index (HDI) and socio-demographic index (SDI) countries, with projections indicating that 25.2 million individuals will be affected by PD by 2050 (Zhu *et al*., 2024; Su *et al*., 2025).

Among the critical molecular targets associated with PD are Leucine-rich repeat kinase 2 (LRRK2), Adenosine A2A receptors, and MAO-B. PD is usually treated by use of levodopa which enhances the amount of dopamine in the brain although prolonged use may result in other complications which include dyskinesia and motor fluctuations (Bogetofte *et al*., 2020). The significant process in PD is the synthesis of 3, 4-dihydroxyphenylacetaldehyde (DOPAL), which is a poisonous product of dopamine metabolism and catalyzed by monoamine oxidase (MAO) (Jinsmaa *et al*., 2011). DOPAL accumulation is proposed to be involved with dopaminergic neuron degeneration, one of the pathological hallmarks of PD. DOPAL synthesis will be reduced by inhibiting MAO, most specifically the MAO-B isoform, which provides neuroprotection as well as may slow the progression of the disease. MAO-B inhibitors include selegiline and rasagiline, which cause the dopamine to be preserved by inhibiting its breakdown in the brain hence increasing its availability. These inhibitors, though effective, have side effects such as agitations, insomnia, and in extreme cases, hypertensive problems due to the interaction with levodopa (Mishal *et al*., 2023). LRRK2 is another protein that can be targeted in the treatment of PD. The kinase triggers mitochondrial dysfunction, oxidative stress, and neuroinflammation, all of which contribute to neuronal death when mutated (for example, G2019S)(Yao *et al*., 2024). Notably, long-term inhibition of LRRK2 activity has been shown to reduce α-synuclein oligomers without causing negative effects in preclinical models, making it a promising target for therapeutic intervention (Ho *et al*., 2022). The Adenosine A2A receptor, another important target, modulates dopaminergic neurotransmission in the basal ganglia through its antagonistic interactions with dopamine D2 receptors (Zhao *et al*., 2024). Blocking A2A receptors has been found

to enhance dopaminergic signaling and alleviate motor symptoms associated with PD (Cenci *et al*., 2022; Waggan *et al*., 2023).

The complexity of this disorder makes it difficult to be treated with a single-target drug, which is why there is an urgent need to explore multi-targeted therapeutic approach. Natural products, with their inherent structural diversity and plethora bioactive compounds that may have anti-inflammatory, antioxidant, and neuroprotective effects (Malar *et al*., 2020; Osonuga *et al*., 2020; Adeyanju *et al*., 2022; Okwute *et al*., 2023; Adegbesan *et al*., 2024; Olalekan *et al*., 2024a; Olalekan *et al*., 2024b; Olalekan *et al*., 2024c), are well positioned to address this challenge. Several plant-derived polyphenols and alkaloids have been shown to modulate oxidative stress pathways, prevent enzymes of the monoamine oxidase network, and suppress neuroinflammatory processes that lead to Parkinson disease. It is these multifunctional characteristics that render natural compounds especially an appealing source in the search of multi-targeted therapeutic approaches that have the capability to tackle the integrated and interconnected pathological processes underlying neurodegeneration (Herraiz & Guillén, 2018; Gahtani *et al*., 2024). In particular, *Camellia sinensis* (Green tea), whose leaves are brewed for thousands of years to make tea, has shown promising neuroprotective effects in various PD models. The tea leaves are a natural source of many beneficial phytochemicals, including the family of catechin polyphenols. Studies have shown that green tea extract mitigate oxidative stress, modulate inflammatory responses, and enhance dopaminergic activity (Malar *et al*., 2020). Additionally, epidemiological studies suggest that higher intake of this beverage is linked to a lower risk of PD progression, highlighting its potential therapeutic value (Li *et al*., 2022).

While this is promising, and it seems to work, the operations behind this observation remain largely unexplored and some pertinent questions are unanswered. Which specific phytochemicals are the key responsible for its positive effect? How do they interact with specific pathological targets such as LRRK2, A2AR, and MAO-B? Do their electronic properties favor stable and selective binding? And are they sufficiently drug-like to warrant further therapeutic development? To provide answers to these, moving from observational data to molecular-level insight is therefore required. This is where computational chemistry offers a powerful and transformative framework.

More specifically, DFT studies and structure-based drug design approach allow electronic structure, molecular reactivity and non-covalent interaction patterns that control the interaction between ligands and proteins to be investigated. Also, DFT studies can be employed to investigate the physicochemical factors that affect the binding affinity, stability, and selectivity by assessing frontier molecular orbitals (HOMO–LUMO), global reactivity descriptors, charge distribution, and intramolecular electron delocalization (Sert *et al*., 2024; Badeji *et al*., 2025; Oladipo *et al*., 2025c; Ekoro & Odeja, 2026). Computational chemistry, together with the molecular docking, molecular dynamics simulations and free-energy calculations, fills the gap between the macroscopic biological observations and the atomic-scale mechanistic interpretation (Durrant & McCammon, 2011; Salmaso & Moro, 2018; Salo-Ahen *et al*., 2020). One such example is the report on the use of computational approach to investigate the inhibitory potential against MAO-A and MAO-B, the enzymes which plays a crucial role in the pathophysiology of Parkinson's disease of halogenated quinoline derivatives (Oladipo *et al*., 2025b). The study reveals how electronic properties and binding interactions govern inhibitory strength. More recently, the structure-guided discovery of marine natural products as glucokinase activators for type 2 diabetes mellitus was investigated via computational studies. The findings showed that the investigated marine natural products (MNP) are potential glycokinase activators for the treatment of type 2 diabetes mellitus. More so, MM/GBSA, ADMET, and DFT analysis confirmed the drug-likeness and therapeutic potential of the selected MNPs. MD and FEL analysis revealed enhanced binding stability of the identified MNPs compared to the native glycokinase ligand (Krishnakumar *et al*., 2026). Hence, computational chemistry is not simply a predictive tool of binding affinity, but rather shed light on the molecular principles in which biological activity is based. By integrating docking, molecular dynamics, MM/PBSA free-energy estimation, ADME profiling and DFT studies, the systematic replacement of empirical findings about neuroprotection with a more mechanistically informed structure-based lead identification becomes possible. This study therefore aim to provide the clarity needed through detailed *in-silico* investigation of the primary bioactive phytochemicals in *Camellia sinensis*, identifying potential multi-target neuroprotective scaffolds against Parkinson's disease and establishing a molecular foundation for subsequent experimental validation.

To achieve this, an integrated computational framework comprising molecular docking, molecular dynamics, MM/PBSA binding free energy analysis, quantum chemical calculations, and pharmacokinetic profiling were employed. It is hoped that this study would provide a robust theoretical foundation for the neuroprotective role of tea phytochemicals, identify lead candidates for further in-vitro and in-vivo research, and enhance the development of effective therapies for PD.

MATERIALS AND METHODS

Target Selection and Protein Preparation

In this work, Leucine-rich repeat kinase 2 (PDB: 8SMC) (Zhu *et al*., 2023), the chain A of adenosine A2A receptor (PDB: 8GNG) (Ohno *et al*., 2023) and Monoamine Oxidase B (PDB: 2BYB) (De Colibus *et al*., 2005) were selected as proteins for Parkinson-relevant molecules of interest to dock and simulate molecular dynamic simulations. This is because they are well-validated druggable proteins involved in dopaminergic dysfunction, neuroinflammation, and dopamine metabolism (Finberg, 2010; Paton, 2020; Jennings *et al*., 2022; Tan *et al*., 2022). DNL-201 was used as the reference ligand of LRRK2 since it is a clinically relevant and highly specific LRRK2 kinase inhibitor that has progressed to clinical studies in Parkinson disease and demonstrated central nervous system penetration, which makes it a good candidate in the study of the inhibitory potential of LRRK2 (Jennings *et al*., 2022). Istradefylline was taken as a representative drug against adenosine A2A receptor because this drug is an FDA-approved antagonist of the A2AR that has been clinically employed as an adjunct therapy to improve motor symptoms of the Parkinson syndrome through the regulation of dopaminergic signaling (Paton, 2020). Rasagiline was employed as the reference inhibitor for MAO-B due to its proven clinical application as a selective and irreversible MAO-B inhibitor that decreases dopamine breakdown and is used as a standard comparator in computational and experimental studies of MAO-B inhibition (Finberg, 2010; Tan *et al*., 2022). These proteins were obtained from the RCSB protein databank using Maestro 12.8 version of the Schrodinger Suite.

Ligand Preparation

The Protein Preparation Wizard was used to preprocess these proteins, which involved adding hydrogens, assigning bond orders, and using the Epik (Shelley *et al*., 2007) to set the protonation state at pH 7.0 ± 2.0. Subsequently, the phytochemicals gotten from a study as shown in Table 1 (Zhao *et al*., 2022), were downloaded from PubChem as well as the reference drugs viz; DNL 201 (CID: 69093374) for leucine-rich repeat kinase 2 (LRRK2), istradefylline (CID: 5311037) for adenosine A2A receptor (A2AR), and rasagiline (CID: 3052776) for monoamine oxidase B (MAO-B), all gotten from PubChem and prepared using the LigPrep wizard of the Suite with OPLS4 Force Field (Jacobson *et al*., 2004).

Molecular Docking Procedure

Molecular docking, which is a computational tool that models the interactions between ligands and protein targets, aids in the interpretation of experimental data (Oladipo *et al*., 2024; Oladipo *et al*., 2025a). Docking was performed using Glide with receptor grid parameters outlined in Table 1 (Friesner *et al*., 2004). It should be noted that grid definition was centered on co-crystallized ligand binding sites and key binding residues within the active pocket. Co-crystallized ligands were used to overlay the resulting complexes onto X-ray structures. Protein-ligand interactions were examined using Discovery Studio 2021 Client. The 25 phytochemicals present in *Camellia sinensis* include Cyanidin, kaempferol-3-galactoside, Catechin, Malvidin, Epigallocatechin, Myricetin-3-galactoside, Myricetin-3-glucoside, Gallic Acid, Quercetin-3-rhamnosylglucoside, Epigallocatechin_gallate, Quercetin-3-glucoside, Pelargonidin, Petunidin, Epicatechin, Chlorogenic Acid, Quercetin-3-galactoside, p-Coumaric acid, Epicatechin gallate, Caffeic Acid, Ellagic Acid, Caffeine, Theophylline, Myricetin 3-rhamnoside-7-glucoside, Quinic acid, and Theobromine. Their PubChem ID is presented in the Appendix (Table S1).

Table 1: The Grid Box Dimensions for the Proteins Docked in this Study

Protein Target		X	Y	Z
LRRK2 (8SMC)	Center	173.59	214.98	-1.94
	Dimensions (Å)	20.00	20.00	20.00
A2AR (8GNG)	Center	102.74	101.60	79.87
	Dimensions (Å)	20.00	20.00	20.00
MAO-B (2BYB)	Center	52.56	156.3	26.1
	Dimensions (Å)	20.00	20.00	20.00

Molecular Dynamics (MD) Simulation of the Receptors and the Optimal Ligand Candidate

Molecular dynamics simulations were executed using Amber 18 (GPU version) with the FF18SB force field systems (Nair & Miners, 2014). ANTECHAMBER's General Amber Force Field and Restrained Electrostatic Potential algorithms were employed to assign ligand atomic charges (Wang *et al*., 2004). To neutralize the system, counter ions (Cl^- and Na^+) were added via LeaP, and the complexes were solvated in TIP3P water molecules within a truncated octahedral box (8 Å buffer). Energy minimization was performed in two phases: first, 1000 steps of steepest descent, 1000 steps of conjugate gradient minimization with the protein fixed (force constant: 500 kcal mol^{-1} $Å^{-2}$), and finally, another 1000 steps each with the protein free. Under NVT conditions with weak restraints (10 kcal mol^{-1} $Å^{-2}$), the system was then heated to 300 K over 50 ps. Under NPT conditions (300 K, 1 atm), the equilibration with Langevin dynamics (collision frequency: 1 ps^{-1}) and isotropic position scaling (relaxation time: 2 ps) was conducted for 500 ps (Loncharich *et al*., 1992). The 100 ns simulation used a 2 fs time step, and cpptraj in Amber18 was used to analyze the results. The AMBER 18 package and the CPPTRAJ script were employed to examine the radius of gyration (RoG), the root mean square deviation (RMSD) of the protein-ligand complexes and the ligands in the binding pocket, and the root mean square fluctuation (RMSF). The OriginPro program was also employed to analyse and visualise the raw data (Seifert, 2014).

MM/PBSA Binding Free Energy Calculation

To calculate the values of free binding energy, the Molecular Mechanics/Poisson-Boltzmann Surface Area method (MM/PBSA) was used to estimate and compare the binding affinities of the systems between the protein and the ligand. The average binding free energy was calculated on 100,000 snapshots from the 100 ns trajectory. The calculated free binding energy (G) of each species of the molecule (complex, ligand, and receptor) may be expressed in the following manner:

$$G_{complex} - (G_{receptor} + G_{ligand}) = \Delta G_{bind} \quad (1)$$

$$(\Delta E_{gas} + \Delta G_{sol}) - T\Delta S = \Delta G_{bind} \quad (2)$$

$$\Delta E_{vdw} + \Delta E_{int} + \Delta E_{elec} = \Delta E_{gas} \quad (3)$$

$$\Delta G_{SA} + \Delta G_{GB} = \Delta G_{sol} \quad (4)$$

$$\gamma SASA = \Delta G_{SA} \quad (5)$$

The gas-phase energy is called the E_{gas} and it is the sum of the internal energy (E_{int}), electrostatic energy (E_{elec}) and Van der Waals energy (E_{vdw}), determined directly as the result of the FF14SB force field. The energy of solvation (G_{sol}) is determined from polar (G_{GB}) and non-polar (G_{SA}) contributions. G_{SA} can be calculated from the solvent-accessible surface area (SASA) with a water probe radius of 1.4 A, and by solving the GB equation, which considers the Gibbs-Bogoliubov variational principle to approximate the free energy of complex molecular systems in molecular dynamics, G_{GB} can be obtained (Kuzemsky, 2015). The temperature is denoted by T, and the total solute entropy by S.

Pharmacokinetics and Drug-Likeness Analysis

Some of the compounds can also react with several classes of molecules and produce a false positive response (Dahlin *et al*., 2015). To deal with this issue, searching of these compounds that are referred to as PAINS (pan assay interference) was conducted through the use of false positive remover software. Upon verification, none of our ligands possess this characteristic. Thereafter, the outcome of the docking and dynamic simulation studies led to the estimation of the physicochemical, pharmacokinetics of our ligands of interest using SwissADME (Daina *et al*., 2017). In order to test these drug-likeness properties, the SMILES format of the candidate molecule was entered into the online server's input plane.

Quantum Chemical Calculations

All quantum chemical calculations in this study were conducted via the Gaussian 16 software package (Frisch *et al*.,

2016) employing the DFT method,wB97X-D functional, a long-range corrected hybrid density functional that incorporates empirical dispersion corrections, to carefully account for non-covalent interactions (Yang *et al*., 2010). The def2-TZVP basis set was applied throughout, ensuring a balanced treatment of electron correlation and basis set convergence for geometry and electronic structure optimization (Weigend, 2006). Geometry optimization and frequency calculations were carried out using a restricted spin formalism for closed-shell systems (Kotaru *et al*., 2022). The vibrational frequencies from the frequency calculations showed that the structures correspond to true energy minima with no imaginary frequencies. Infrared vibrational modes were analyzed to confirm structural stability and identify characteristic functional group motions. Visualization and analysis of molecular orbitals, including HOMO–LUMO plots, were performed using GaussView 6.0 (Dennington *et al*., 2023) and Chemcraft (Andrienko, 2010). Natural Bond Orbital (NBO) analysis was conducted through the NBO module 7.0 integrated within Gaussian 16 (Glendening *et al*., 2019). Key donor–acceptor interactions and second-order perturbation energies were extracted and interpreted to assess electronic delocalization and intramolecular stabilization. Molecular Electrostatic Potential (MEP) surfaces were generated to analyze the spatial distribution of electrostatic charges on molecular surfaces (Suresh *et al*., 2022). These MEP maps were compared with electrophilicity indices derived from frontier molecular orbital (FMO) analysis to evaluate electronic polarization and predict molecular interaction profiles. In addition to FMO analysis, a set of global quantum chemical descriptors was computed to quantify the reactivity, stability, and electron transfer characteristics of the complexes (Huang *et al*., 2017). The energy gap (ΔE) was calculated as the difference between the energy values of the HOMO and LUMO, i.e., $\Delta E = E_{LUMO} - E_{HOMO}$ (Badeji *et al*., 2024). The electron affinity (EA) and ionization potential (IP) were defined as $EA = -E_{LUMO}$ and $IP = -E_{HOMO}$, respectively, representing the energetic costs of removing and adding an electron (Houk, 1977; Zhan *et al*., 2003). The chemical hardness (η) was derived using the expression $\eta = (IP - EA)/2$, while the chemical softness (σ) was calculated as the multiplicative inverse of hardness ($\sigma = 1/\eta$) (Pearson, 2005; Franco-Pérez *et al*., 2018). Electronegativity, denoted by χ, representing the tendency of a species to attract electrons(Parr *et al*., 1978; Pal & Chattaraj, 2023), was calculated as $\chi = (IP + EA)/2$. The chemical potential, denoted by μ, was taken as the negative value of electronegativity, $\mu = -\chi = -(IP + EA)/2$, reflecting the tendency of electrons to escape from the system (Datta *et al*., 2013). Then, the electrophilicity index (ω) was evaluated using the formula $\omega = \mu^2 / (2\eta)$, which quantifies the stabilization energy a molecule undergoes upon acquiring electronic charge from the environment (Pal & Chattaraj, 2023).

RESULTS AND DISCUSSION

Molecular Docking Analysis

The docking results for the *Camellia sinensis* phytochemicals and the reference drugs are presented in Appendix *Table S1*. The superimposition of the co-crystallized and docked complexes is presented in Figure 1. The molecular docking results showed that some of the phytochemicals demonstrated stronger binding scores compared to those of the reference drugs, indicating favorable binding pose within the active sites of LRRK2, A2AR, and MAO-B. The protein-ligand interaction plots, which illustrated the key hydrogen bonding, π-π stacking, and hydrophobic interactions in the protein binding complexes, shed light into the molecular interactions and predicted inhibition potential of the complexes, especially those with higher binding energies to the proteins.

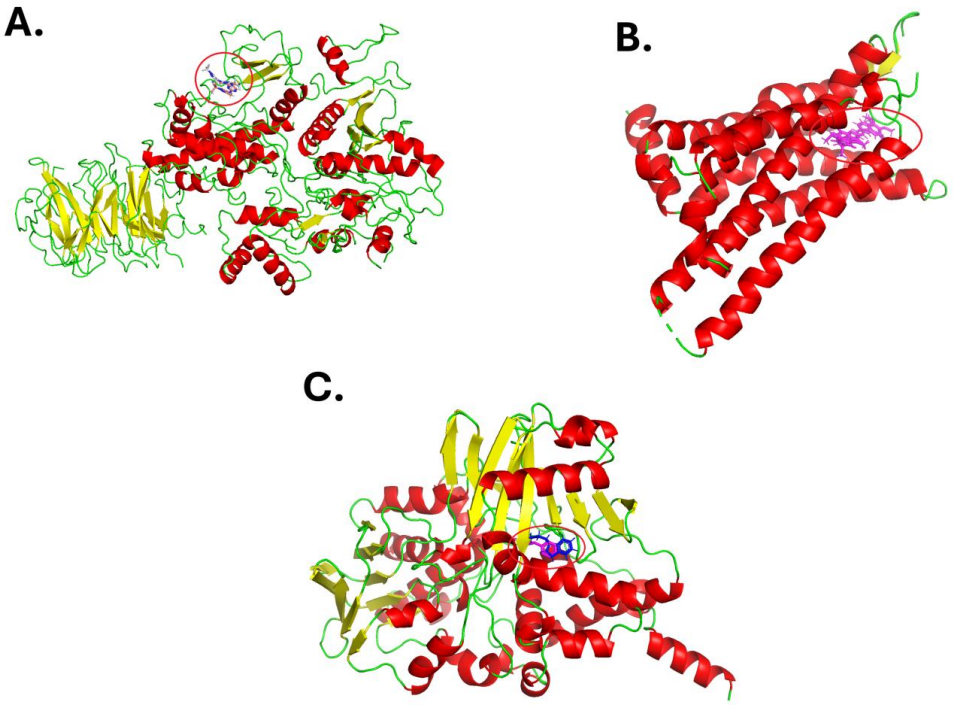

Figure 1: Ribbon Representation (α-helices: red, β-sheets: Yellow, Loops: green) of the Superimposed Ligands in the Binding powhacket of (A.) Leucine-rich Repeat kinase 2 (B.) Adenosine A2A Receptor and (C.) Monoamine Oxidase B, with Ligands Displayed in Stick Style (Circled)

Docking Interaction Analysis

The plots of protein-ligand interaction were produced to provide clarity on the interactions between the reference drug and the phytochemicals of interest with the amino acid residues in the binding pocket of the protein. These plots are shown in Figures 2-4. The reference drug DNL-201 exhibited strong interactions with LRRK2 through multiple binding forces. It formed hydrogen bonds with LYS498, LEU541, ALA542, and ASP609, contributing to its stability within the binding site. Additionally, alkyl/π-alkyl interactions were observed with LEU477, ALA496, MET539, LEU541, and LEU593, while a π-sigma bond was identified with VAL485. Further, Van der Waals interactions were established with SER546, GLY545, ARG487, ILE525, GLU540, ALA608, TYR610, HID590, and ARG549, reinforcing the binding stability.

Among the phytochemicals, Caffeine formed hydrogen bonds with GLU540, LEU541, ALA542, and HID590, similar to DNL-201, while also engaging in alkyl/π-alkyl interactions with LEU477, VAL485, ALA496, MET539, LEU593, and ALA608. It further established Van der Waals interactions with GLU545, SER546, GLY478, ASP609, and ILE525. Theobromine, a structurally similar methylxanthine, interacted with LEU477, LEU541, and ALA542 through hydrogen bonding, alongside alkyl/π-alkyl interactions with VAL485, ALA496, ILE525, and LEU593 and Van der Waals interactions with GLY478, GLU540, GLY545, and SER546. Epicatechin demonstrated strong interactions, forming hydrogen bonds with GLU540, GLY478, ASP479, and HID590. It participated in alkyl/π-alkyl interactions with VAL485, ALA496, LEU593, and ALA608 and displayed a π-sulfur bond with MET539. Additional Van der Waals interactions with LEU541, ALA542, ASN591, LEU477, GLY480, LYS498, ASP609, and ILE525 contributed to its binding affinity. Cyanidin, another flavonoid, formed hydrogen bonds with ASP479, LYS498, GLU540, and ALA542, π-alkyl interactions with LEU477, ALA496, and LEU593, and a π-sigma bond with VAL485, supported by Van der Waals interactions with GLY480, GLY478, HID590, LEU541, ILE525, and MET539.

Among the strongest binders, Petunidin interacted through hydrogen bonds with GLU540 and ASP609, alkyl/π-alkyl interactions with ALA496, LEU593, LEU477, and VAL485, and a π-π stacked interaction with HID590. Further Van der Waals interactions with ILE525, MET539, GLY478, ASP479, LYS588, ASN591, SER546, GLY545, ALA542, and LEU541 reinforced its strong binding affinity.

In relation with A2AR, the reference drug Istradefylline formed hydrogen bonds with PRO1, MET3, and ASN231, indicating a strong anchoring mechanism. Additionally, it exhibited alkyl/π-alkyl interactions with ILE65, LEU84, LEU227, LEU245, and MET248. Notably, it interacted with PHE155 and TYR249 in a π-π stacked and π-π T-shaped manner, which may enhance its stability, alongside Van der Waals interactions with PHE61, ALA80, ILE79, ALA62, ILE252, SER66, LEU154, ILE230, MET164, ALA87, HID228, and VAL83.

Among the phytochemicals, Epigallocatechin demonstrated strong binding through hydrogen bonds with SER66, VAL83, GLU156, and ASN231, and also alkyl/π-alkyl interactions with VAL83, PHE155, and ILE252. It further engaged in π-π stacked bonding with PHE155 and a π-sulfur bond with MET248, with additional Van der Waals interactions involving LEU84, LEU154, LEU245, ILE65, ALA62, SER255, ALA58, LEU86, TRP224, and LEU227. Pelargonidin, in contrast, formed hydrogen bonds with ALA62 and SER66, a π-alkyl interaction with ILE252, and a π-sulfur bond with MET248, alongside Van der Waals interactions with ILE63, ILE65, LEU227, ASN231, ILE230, TYR249, LEU245, and LEU154.

As for MAO-B, The reference drug Rasagiline interacted through hydrogen bonds with LEU169, ILE196, and GLN204, while also displaying alkyl/π-alkyl interactions with TYR396, TYR58, PHE341, ILE314, CYS170, TYR324, and ILE197. Notably, it exhibited π-π T-shaped and π-cation interactions with TYR324, alongside Van der Waals interactions with TYR433, LEU343, and PHE166.

For cyaniding, hydrogen bond was formed with PRO100, CYS170, ILE196, and TYR396, as well as π-alkyl interactions with LEU169 and CYS170. More so, it engaged in a π-π T-shaped interaction with TYR324 and Van der Waals interactions with TYR433, GLN204, SER198, THR199, THR312, LEU86, PHE97, GLY99, PHE101, ILE314, PHE166, and ILE197. Similarly, Malvidin interacted through hydrogen bonds with PRO100, LEU162, CYS170, and ILE197, alkyl/π-alkyl interactions with LEU86, LEU169, and ILE314, and π-π T-shaped and π-sulfur bonds with TYR324 and CYS170, respectively. Additional Van der Waals interactions with ILE196, TYR433, TYR396, TYR58, PHE341, MET339, GLN204, SER198, THR199, THR312, GLY99, PHE97, PHE101, LEU165, PHE166, and TRP117 enhanced its binding stability.

Pelargonidin exhibited hydrogen bonds with GLY56, LEU169, and CYS170, π-alkyl and π-π interactions with LEU169, TYR396, and TYR324, and a π-sulfur bond with CYS170, with Van der Waals interactions involving SER57, TYR58, PHE341, MET339, GLN204, ILE314, ILE197, PHE166, ILE196, and TYR433. Petunidin formed hydrogen bonds with GLN204, THR199, PRO100, ILE196, ILE197, and TYR433, π-alkyl and π-π interactions with LEU169 and TYR324, and a π-sulfur bond with CYS170. Additional Van der Waals interactions with GLY56, TYR58, LEU326, SER198, THR312, LEU86, PHE97, GLY99, ILE314, LEU162, PHE101, TRP117, PHE166, TYR186, and TYR396 further stabilized the complex.

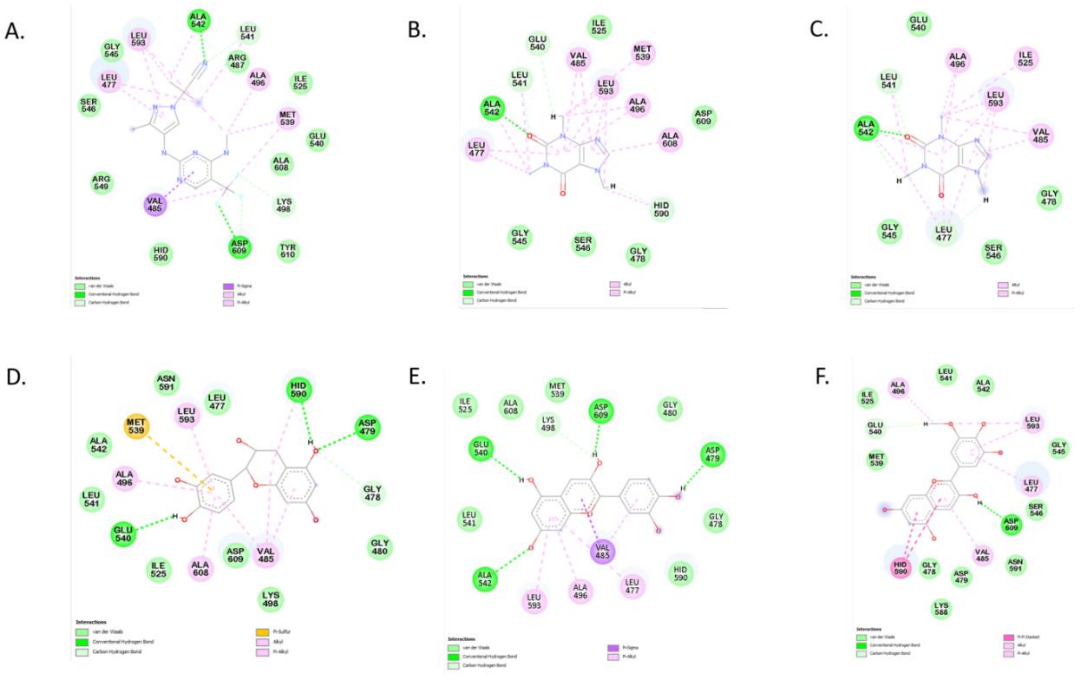

Figure 2: Two-dimensional Interaction Plots of Protein-ligand Interactions of
A. LRRK2 + DNL201 B. LLRK2 + Caffeine C. LRRK2 + Theobromine
D. LRRK2 + Epicatechin E. LRRK2 + Cyanidin F. LRRK2 + Petunidin

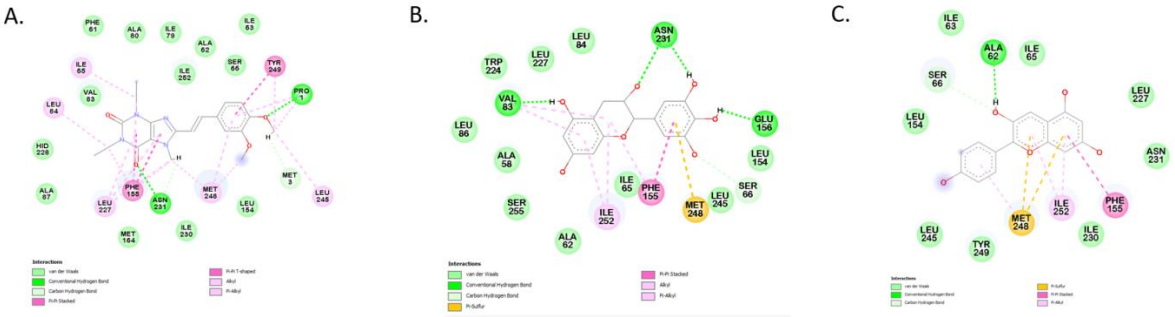

Figure 3: Two-dimensional Interaction Plots of Protein-ligand Interactions of
A. A2AR + Istradefylline B. A2AR + Epigallocatechin C. A2AR + Pelargonidin

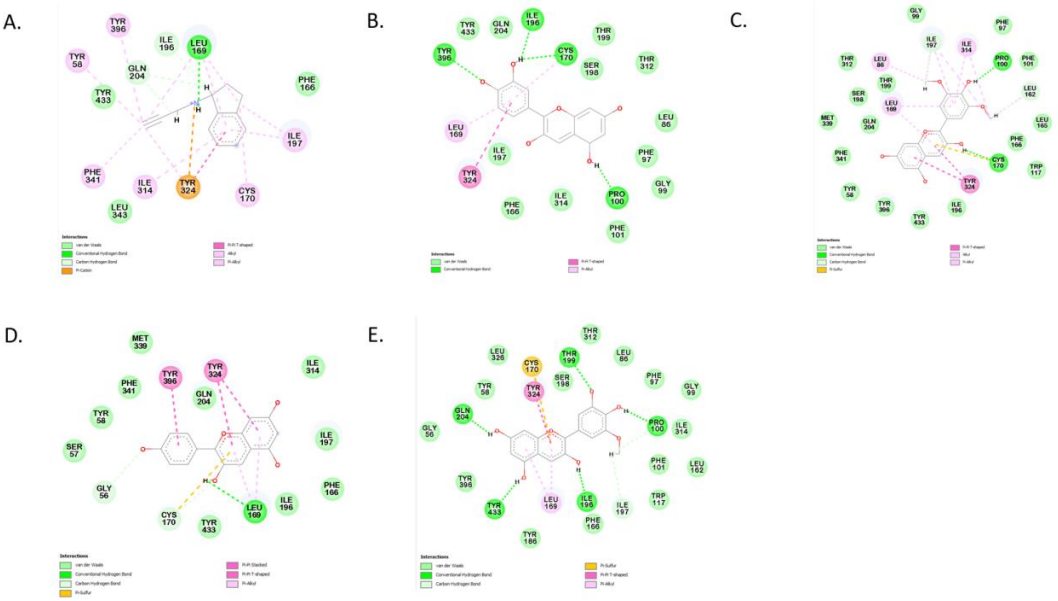

Figure 4: Two-dimensional Interaction Plots of Protein-ligand Interactions of A. MAO-B + Rasagiline; B. MAO-B + Cyanidin; C. MAO-B + Malvidin; D. MAO-B + Pelargonidin; E. MAO-B + Petunidin

Molecular Dynamic (MD) Simulation and Structural Stability Analysis

To further validate the stability of the top-ranked docking complexes, the selected phytochemicals of interest and the reference ligands complexes underwent a 100 ns molecular dynamic simulation. Considering that molecular docking mainly evaluates the geometrical position of the molecules within the active site of any protein, MD simulations were carried out on the promising phytochemicals in the *Camellia sinensis* as well as of reference drug complexes to study their conformational stability, interaction persistence, and also to conduct a more comprehensive structural analysis under physiological conditions (Obakachi *et al*., 2022; Oladipo *et al*., 2024; Olalekan *et al*., 2024b).

Moreover, the inspection of the protein backbone RMSD and ligand positional stability indicated that all complexes attained a stable conformational regime after an initial equilibration period, with no evidence of long-term structural drift over the remainder of the 100 ns simulations. To evaluate the structural stability and conformational changes of the protein-ligand complexes in this study, RMSF of alpha-carbon (Cα) atoms, RMSD and RoG were analyzed. These parameters provide insights into protein flexibility and compactness, which may impact biological activity. The computed mean values for LRRK2, A2AR, and MAO-B complexes are presented in Table 2 and Figure 5.

Table 2: Computed Mean Values of Parameters Utilized to Assess the Structural Stability of the Protein Complexes

Computed Mean Values of Parameters Employed to Assess the Structural Stability of LRRK2 Complexes			
Complex	**RMSD (Å)** **Mean ± SD**	**RoG (Å)** **Mean ± SD**	**RMSF (Å)** **Mean ± SD**
LRRK2 (APO)	4.443 ± 1.073	38.836 ± 0.231	5.886 ± 2.153
LRRK2 + DNL201	4.163 ± 0.678	38.945 ± 0.324	5.336 ± 1.714
LRRK2 + Caffeine	5.097 ± 1.073	40.109 ± 0.329	6.413 ± 2.165
LRRK2 + Theobromine	4.789 ± 0.903	39.515 ± 0.260	4.477 ± 1.409
LRRK2 + Epicatechin	3.969 ± 0.673	39.674 ± 0.220	4.879 ± 1.568
LRRK2 + Cyanidin	4.020 ± 1.025	38.560 ± 0.446	9.286 ± 3.288
LRRK2 + Petunidin	3.369 ± 0.564	38.454 ± 0.269	6.074 ± 2.043
Computed Mean Values of Parameters Employed to Assess the Structural Stability of A2AR Complexes			
Complex	**RMSD (Å)** **Mean ± SD**	**RoG (Å)** **Mean ± SD**	**RMSF (Å)** **Mean ± SD**
A2AR (APO)	3.087 ± 0.740	21.008 ± 0.161	11.429 ± 4.245
A2AR + Istradefylline	2.383 ± 0.352	20.940 ± 0.140	10.173 ± 4.191
A2AR + Epigallocatechin	2.948 ± 0.554	20.960 ± 0.144	9.165 ± 3.639
A2AR + Pelargonidin	3.085 ± 0.670	21.055 ± 0.111	10.841 ± 4.086
Computed Mean Values of Parameters Employed to Assess the Structural Stability of MAO-B Complexes			
Complex	**RMSD (Å)** **Mean ± SD**	**RoG (Å)** **Mean ± SD**	**RMSF (Å)** **Mean ± SD**
MAO-B (APO)	2.074 ± 0.372	23.399 ± 0.080	8.220 ± 2.811
Rasagiline	1.654 ± 0.209	23.410 ± 0.073	9.689 ± 3.533
Cyanidin	2.316 ± 0.257	23.616 ± 0.093	9.231 ± 3.442
Malvidin	2.109 ± 0.315	23.621 ± 0.088	6.839 ± 2.260
Pelargonidin	2.012 ± 0.318	23.399 ± 0.084	7.892 ± 2.893
Petunidin	1.840 ± 0.287	23.522 ± 0.096	11.701 ± 4.498

The binding of phytochemicals in *Camellia sinensis* to LLRK2, A2AR and MAO-B resulted in varying levels of structural stability, as indicated by the computed mean values of RMSF, RMSD, and RoG parameters.

For LRRK2, the RMSD values, which indicate overall stability, showed that the APO (unbound) LRRK2 exhibited an average deviation of 4.443 ± 1.073 Å. Upon binding, DNL-201, the reference drug, led to a slight stabilization with an RMSD of 4.163 ± 0.678 Å, suggesting that ligand binding restricted excessive conformational shifts. Among the phytochemicals, Epicatechin and Petunidin showed the most stability, with RMSD values of 3.969 ± 0.673 Å and 3.369 ± 0.564 Å, respectively, indicating their ability to enhance structural rigidity upon binding. Caffeine and Cyanidin, on the other hand, resulted in increased structural fluctuations, with RMSD values of 5.097 ± 1.073 Å and 4.020 ± 1.025 Å, respectively, suggesting greater flexibility in the LRRK2 binding pocket.

The RoG, which measures the compactness of the protein, remained largely stable across all complexes, with values ranging from 38.454 Å (Petunidin) to 40.109 Å (Caffeine). Notably, Cyanidin (38.560 Å) and Petunidin (38.454 Å) resulted in a slightly more compact structure compared to the APO LRRK2 (38.836 Å), indicating a potential stabilizing effect.

The RMSF, which reflects residue-level flexibility, varied significantly among ligands. Cyanidin exhibited the highest RMSF (9.286 ± 3.288 Å), suggesting localized instability, while Theobromine (4.477 ± 1.409 Å) and Epicatechin (4.879 ± 1.568 Å) contributed to reduced fluctuations, indicative of stronger residue-specific stabilization. Petunidin (6.074 ± 2.043 Å) also showed moderate stabilization while retaining some flexibility.

For A2AR, the APO form had an RMSD of 3.087 ± 0.740 Å, suggesting moderate flexibility. Upon ligand binding, Istradefylline, the reference drug, demonstrated the highest stabilization effect, reducing RMSD to 2.383 ± 0.352 Å, which implies a significant reduction in backbone fluctuations. Among the phytochemicals, Epigallocatechin (2.948 ± 0.554 Å) maintained stability comparable to the APO form, while Pelargonidin (3.085 ± 0.670 Å) resulted in slightly higher fluctuations, similar to the unbound protein.

The RoG values across all A2AR complexes remained consistent, with minimal variations. The APO structure had a

RoG of 21.008 ± 0.161 Å, while bound complexes ranged between 20.940 ± 0.140 Å (Istradefylline) and 21.055 ± 0.111 Å (Pelargonidin), suggesting that ligand binding did not significantly alter the overall protein compactness.

The RMSF values indicated higher fluctuations in the APO form (11.429 ± 4.245 Å), suggesting greater flexibility in the unbound state. Istradefylline (10.173 ± 4.191 Å) slightly reduced these fluctuations, while Epigallocatechin (9.165 ± 3.639 Å) showed even lower fluctuations, suggesting that it may contribute to enhanced stability. Pelargonidin (10.841 ± 4.086 Å), however, maintained similar levels of residue flexibility as the APO structure, indicating a weaker stabilizing effect.

The APO MAO-B gave an RMSD of 2.074 ± 0.372 Å for MAO-B, suggesting a comparatively stable structure. Upon ligand binding, Rasagiline, the reference drug, significantly stabilized the protein, reducing RMSD to 1.654 ± 0.209 Å. Among the phytochemicals, Petunidin (1.840 ± 0.287 Å) and Pelargonidin (2.012 ± 0.318 Å) exhibited similar levels of stabilization. Cyanidin (2.316 ± 0.257 Å), on the other hand, resulted in increased deviations compared to the APO form, suggesting a more flexible binding interaction.

The RoG values showed minimal variation, with the APO form at 23.399 ± 0.080 Å and ligand-bound complexes ranging between 23.410 ± 0.073 Å (Rasagiline) and 23.621 ± 0.088 Å (Malvidin). This suggests that the overall compactness of MAO-B was not significantly affected by the ligand binding.

The RMSF values provided insights into residue flexibility, with the APO form exhibiting an average fluctuation of 8.220 ± 2.811 Å. Petunidin (11.701 ± 4.498 Å) resulted in the highest fluctuations, suggesting a more dynamic interaction with MAO-B. Conversely, Malvidin (6.839 ± 2.260 Å) and Pelargonidin (7.892 ± 2.893 Å) demonstrated reduced residue fluctuations, indicating potential stabilization effects. To ensure the reliability of the binding free-energy calculations, the convergence of all molecular dynamics trajectories was carefully assessed prior to MM/PBSA analysis. Consequently, MM/PBSA binding free-energy calculations were performed using snapshots extracted exclusively from the equilibrated portion of each trajectory, thereby ensuring that the reported binding free energies reflect statistically converged and dynamically stable protein–ligand interactions.

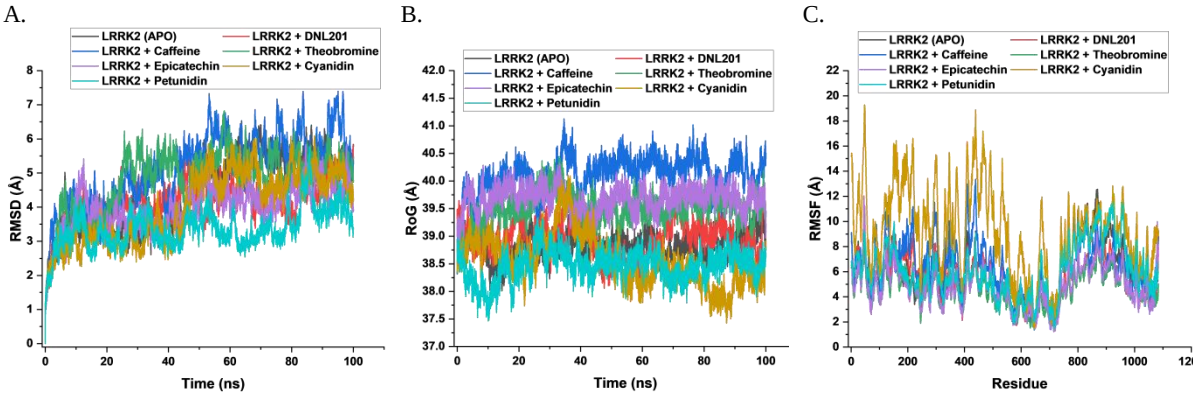

The Comparative A). RMSD B). RoG and C). RMSF Plots of Cα Atoms of the LRRK2 System Computed using 100 ns MD Simulations

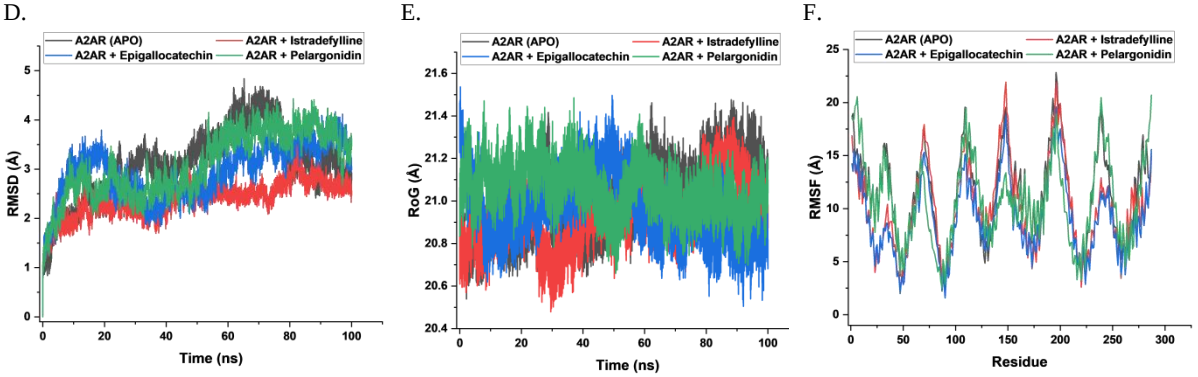

The Comparative D). RMSD E). RoG and F). RMSF Plots of Cα Atoms of the A2AR System Computed using 100 ns MD Simulations

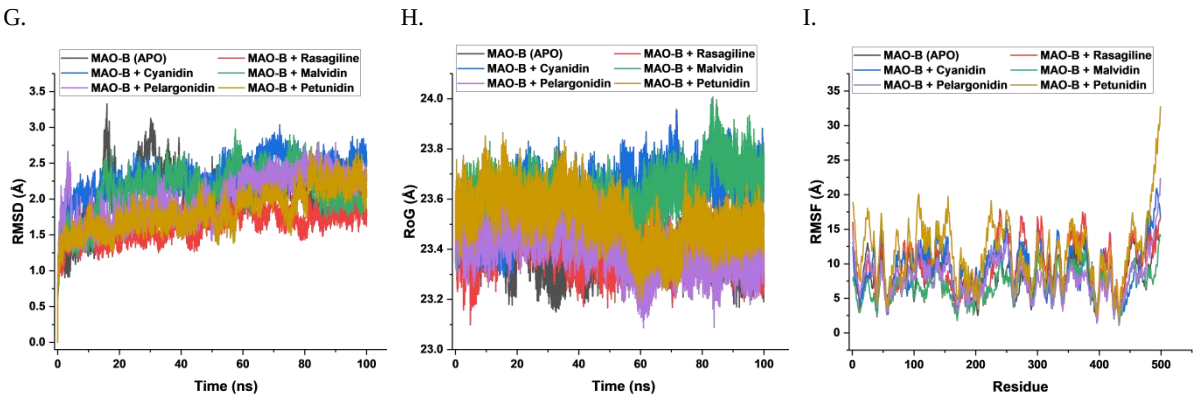

The Comparative G). RMSD H). RoG and I). RMSF Plots of Cα Atoms of the MAO-B System Computed using 100 ns MD Simulations

Figure 5: Comparative RMSD, RoG, and RMSF Plots of Cα Atoms in the Protein Systems, Computed using 100 ns MD Simulations

Binding Free Energy Evaluation via MM/PBSA Analysis

We employed the MM/PBSA computational method reported by Ylilauri and Pentikäinen in 2013, to compute the binding free energies (ΔG_{bind}) between the protein/enzyme and the ligand (Ylilauri & Pentikäinen, 2013). 100 ns molecular dynamic simulations was carried out on the molecules after which the binding energy of the phytochemicals of interest and referenced drugs at the active sites of proteins were estimated. The thermodynamic binding free energy profiles of *Camellia sinensis* phytochemicals and reference drugs towards the three proteins examined in this study viz: LRRK2, A2AR, and MAO-B are demonstrated by the results described in Table 3. The binding free energy profiles of selected *Camellia sinensis* phytochemicals and reference drugs with LRRK2, A2AR, and MAO-B reveal significant variations in their binding affinities. Among the LRRK2 inhibitors, DNL-201, a reference drug, show a binding free energy (ΔG_{bind}) of -27.31 kcal/mol, while several phytochemicals demonstrated even stronger binding affinities. Notably, Petunidin had the highest affinity (ΔG_{bind} = -38.48 kcal/mol), followed by Cyanidin (-31.96 kcal/mol) and Epicatechin (-28.44 kcal/mol), suggesting that these compounds may serve as effective LRRK2 inhibitors. Conversely, Caffeine (-22.42 kcal/mol) and Theobromine (-20.13 kcal/mol) exhibited weaker binding to LRRK2.

Table 3: Thermodynamic Binding Free Energy Profiles for the Phytochemicals of Interest and Reference Drugs with LRRK2, A2AR, and MAO-B

Thermodynamic Binding Free Energy Profiles of *Camellia Sinensis* Phytochemicals of Interest and Reference Drugs to LRRK2, A2AR, and MAO-B					
Complex	**E_{vdw}**	**E_{elec}**	**ΔG_{gas}**	**ΔG_{sol}**	**ΔG_{bind}**
LRRK2					
DNL-201*	-39.2253 ± 2.4420	-4.3978 ± 3.0868	-43.6231 ± 3.4489	16.3103 ± 2.2735	-27.3128± 2.1812
Caffeine	-30.0866 ± 2.3771	-13.4508 ± 3.8067	-43.5375 ± 4.3628	21.1091 ± 2.9678	-22.4284 ± 2.1445
Theobromine	-26.7420 ± 1.9904	-12.7236 ± 3.1915	-39.4656 ± 3.5571	19.3295 ± 2.5443	-20.1361 ± 1.8190
Epicatechin	-35.9286 ± 2.9747	-15.7475 ± 10.3540	-51.6762 ± 9.8845	23.2333 ± 6.2935	-28.4429 ± 4.4017
Cyanidin	-30.0957 ± 3.9098	-158.4867 ± 14.3372	-188.5824 ± 13.1580	156.6259 ± 11.2153	-31.9565 ± 3.5142
Petunidin	-39.4084 ± 3.2449	-182.6134 ± 21.1881	-222.0218 ± 19.8098	183.5385 ± 17.6061	-38.4833 ± 3.9613
A2AR					
Istradefylline*	-59.0800 ± 3.1482	-19.5740 ± 4.2088	-78.6540 ± 5.2720	28.9454 ± 3.7810	-49.7085 ± 3.4461
Epigallocatechin	-41.7042 ± 2.6440	-27.3795 ± 7.7434	-69.0837 ± 7.0284	32.6525 ± 4.2203	-36.4311 ± 3.5824
Pelargonidin	-30.3744 ± 3.4284	-21.6554 ± 15.8108	-52.0298 ± 14.6717	20.4197 ± 11.5760	-31.6101 ± 4.4709
MAO-B					
Rasagiline*	-33.7953 ± 1.9804	-36.1406 ± 7.7994	-69.9359 ± 7.6248	36.4280 ± 6.7001	-33.5079 ± 2.4044
Cyanidin	-35.8088 ± 2.8341	-57.4661 ± 9.1563	-93.2749 ± 8.7378	57.5624 ± 8.3073	-35.7124 ± 2.9253
Malvidin	-50.6237 ± 2.7745	-43.5775 ± 7.3534	-94.2012 ± 7.2974	52.7138 ± 6.4397	-41.4874 ± 3.2867

Thermodynamic Binding Free Energy Profiles of *Camellia Sinensis* Phytochemicals of Interest and Reference Drugs to LRRK2, A2AR, and MAO-B

Complex	E_{vdw}	E_{elec}	ΔG_{gas}	ΔG_{sol}	ΔG_{bind}
Pelargonidin	-40.9317 ± 2.4345	-25.9954 ± 12.1687	-66.9271 ± 11.3500	36.1574 ± 9.1781	-30.7697 ± 3.4723
Petunidin	-41.6937 ± 3.2359	-66.9132 ± 11.9777	-108.6068 ± 11.2738	64.1081 ± 8.9644	-44.4987± 44.4987

***** reference drug

For A2AR, Istradefylline, the reference drug, demonstrated the highest affinity with ΔG_{bind} = -49.71 kcal/mol. Among the phytochemicals, Epigallocatechin (-36.43 kcal/mol) displayed the strongest binding, while Pelargonidin (-31.61 kcal/mol) exhibited moderate binding affinity. These results imply that Epigallocatechin could be a promising candidate for A2AR modulation.

The analysis of MAO-B interactions revealed that Rasagiline, the reference drug, had a ΔG_{bind} of -33.50 kcal/mol. However, Petunidin (-44.49 kcal/mol) exhibited even stronger binding, making it a highly promising MAO-B inhibitor. Additionally, Malvidin (-41.48 kcal/mol) and Cyanidin (-35.71 kcal/mol) also showed high affinities, outperforming Rasagiline.

Multi-target efficiency is a desirable property in drug discovery, as compounds that interact with multiple proteins involved in a disease pathway may provide enhanced therapeutic effects. In this study, Cyanidin displayed strong binding affinities across two major targets: LRRK2 (-31.96 kcal/mol) and MAO-B (-35.71 kcal/mol), suggesting its potential as a dual inhibitor for neurodegenerative diseases. Similarly, Petunidin demonstrated high affinities for both LRRK2 (-38.48 kcal/mol) and MAO-B (-44.49 kcal/mol), making it the most promising multi-target phytochemical.

Comparative Analysis of the Pharmacokinetic and Physicochemical Characteristics of Promising *Camellia Sinensis* Phytochemicals

The pharmacokinetic and physicochemical properties of the selected phytochemicals were assessed using standard drug-likeness criteria, including Lipinski's Rule of Five (Ro5), water solubility (LogS), hydrogen bond donors (HBD), rotatable bonds (RotBs), total polar surface area (TPSA), and hydrogen bond acceptors (HBA). Additionally, key pharmacokinetic parameters, such as P-glycoprotein (P-gp) substrate status, gastrointestinal (GI) absorption, cytochrome P450 (CYP) enzyme inhibition, blood-brain barrier (BBB) permeability, and skin permeability (LogKp), were analyzed to predict the potential bioavailability and metabolic interactions of these compounds. All compounds according to Table 4 showed promise for the development of oral drugs by adhering to the Lipinski's Rule of Five (Ro5). Caffeine (194.19 g/mol) and Theobromine (180.16 g/mol) had the lowest molecular weights (MW), whereas Epicatechin, Cyanidin, Petunidin, Epigallocatechin, Pelargonidin, and Malvidin had slightly higher MWs (ranging from 271.24 g/mol to 331.30 g/mol) but remained below the 500 Da threshold, supporting their drug-likeness.

Lipophilicity, measured as LogP, influences membrane permeability and drug absorption. Caffeine (-0.08) and Theobromine (-0.12) had the lowest lipophilicity, indicating good aqueous solubility but potentially lower membrane permeability. Pelargonidin (0.93), Malvidin (0.92), and Petunidin (0.63) exhibited higher LogP values, suggesting increased lipophilicity, which may enhance passive diffusion across lipid membranes. The total polar surface area (TPSA) values ranged between 61.82 Å² (Caffeine) and 130.61 Å² (Epigallocatechin). Compounds with TPSA ≤ 140 Å² generally have good oral bioavailability, and all tested compounds fell within this range. HBD and HBA were also within the acceptable limits, with all compounds having HBD ≤ 5 and HBA ≤ 10, further supporting their potential for good bioavailability.

Water solubility, measured using LogS values, indicated that Caffeine (-1.48) and Theobromine (-0.98) were highly soluble. Epicatechin (-2.22), Cyanidin (-2.60), and Petunidin (-3.39) were classified as soluble to moderately soluble, while Malvidin (-3.60) and Pelargonidin (-3.49) exhibited lower solubility. High solubility generally correlates with better GI absorption, a crucial factor in oral drug formulation. All tested compounds exhibited high GI absorption, indicating their suitability for oral administration. Nevertheless, it was not predicted that any of the compound examined would penetrate the blood-brain barrier (BBB), suggesting that these phytochemicals may not readily reach the central nervous system (CNS) without structural modifications to enhance permeability. Moreso, they are suitable for peripheral targets in Parkinson's disease.

P-gp substrate status was positive for Epicatechin, Cyanidin, Petunidin, Pelargonidin, and Malvidin, suggesting that these compounds may be susceptible to efflux by P-glycoprotein transporters, potentially limiting their bioavailability. Caffeine and Theobromine were not P-gp substrates, indicating reduced susceptibility to efflux transport. Regarding cytochrome P450 (CYP) enzyme inhibition, Cyanidin, Petunidin, and Pelargonidin inhibited CYP1A2, suggesting potential drug-drug interactions, whereas all other compounds showed no CYP inhibition, indicating a lower likelihood of metabolic interference. Skin permeability (LogKp) values ranged from -6.33 cm/s (Pelargonidin) to -8.17 cm/s (Epigallocatechin), suggesting low skin permeability for all compounds. This implies that transdermal administration may not be a viable route for these molecules, reinforcing their suitability for oral delivery.

The phytochemicals evaluated in this study exhibit favorable physicochemical and pharmacokinetic properties, aligning well with drug-likeness criteria. Caffeine and Theobromine stood out for their high solubility and GI absorption, making them promising for oral administration. Epicatechin, Cyanidin, Petunidin, and Pelargonidin, while also displaying good bioavailability, may require further structural modifications to enhance BBB permeability and reduce P-gp efflux susceptibility. Metabolic interactions, particularly CYP1A2 inhibition by Cyanidin, Petunidin, and Pelargonidin, may need to be addressed in further studies to minimize drug-drug interaction risks.

The predicted toxicity profiles further support the relative safety of the evaluated phytochemicals within acceptable drug-likeness thresholds. Caffeine exhibited the lowest predicted LD_{50} value (127 mg/kg), indicating comparatively higher acute toxicity, consistent with its well-documented dose-dependent stimulant and neuroactive effects. Theobromine showed a substantially higher LD_{50} (837 mg/kg), reflecting lower acute toxicity than caffeine. In contrast, Epicatechin and Epigallocatechin demonstrated very high predicted LD_{50} values (10,000 mg/kg), suggesting minimal acute toxicity risk, while Cyanidin, Petunidin,

Pelargonidin, and Malvidin also displayed relatively high safety margins (3,919–5,000 mg/kg). Importantly, all compounds were predicted to be non-hepatotoxic, indicating a low likelihood of liver injury at therapeutic concentrations. However, neurotoxicity predictions identified Caffeine and Theobromine as active, aligning with their central nervous system stimulatory mechanisms. Carcinogenicity alerts were observed for Cyanidin and Petunidin, warranting cautious interpretation and further experimental validation, although other compounds were predicted inactive in this regard.

These findings support the potential pharmaceutical applications of these phytochemicals, particularly in oral formulations targeting peripheral biological pathways. To validate their therapeutic efficacy and improve their pharmacokinetic profiles, more *in vitro* and in vivo studies are required.

Table 4: Physicochemical and Pharmacokinetic Properties of Selected Phytochemicals in *Camellia Sinensis*

Property	Caffeine	Theobromine	Epicatechin	Cyanidin	Petunidin	Epigallocatechin	Pelargonidin	Malvidin	Acceptable Threshold (Ro5)
Molecular Weight(g/mol)	194.19	180.16	290.27	287.24	317.27	306.27	271.24	331.30	<500 Da
LogP (Consensus)	0.08	-0.12	0.85	0.32	0.63	0.42	0.93	0.92	<5
LogS (ESOL)	-1.48	-0.98	-2.22	-2.60	-3.39	-2.08	-3.49	-3.60	0 to -6
TPSA (Å²)	61.82	72.68	110.38	114.29	123.52	130.61	94.06	112.52	≤140
HBA	3	3	6	6	7	7	5	7	≤10
HBD	0	1	5	5	5	6	4	4	≤5
Rotatable Bonds	0	0	1	1	2	1	1	3	<10
GI Absorption	High	High	High	High	High	High	High	High	
BBB Permeability	No	No	No	No	No	No	No	No	
P-gp Substrate	No	No	Yes	Yes	Yes	No	Yes	Yes	
CYP1A2 Inhibition	No	No	No	Yes	Yes	No	Yes	Yes	
Skin Permeability (LogKp cm/s)	-7.53	-7.95	-7.82	-7.51	-6.88	-8.17	-6.33	-6.73	
Predicted LD_{50} (mg/kg)	127	837	10000	5000	5000	10000	3919	5000	
Hepatotoxicity	Inactive	Inactive	Inactive	Inactive	Inactive	Inactive	Inactive	Inactive	
Neurotoxocity	Active	Active	Inactive	Inactive	Inactive	Inactive	Inactive	Inactive	
Carcinogenicity	Inactive	Inactive	Inactive	Active	Active	Inactive	Inactive	Inactive	

Quantum Chemical Calculations

Geometry Optimization

The optimized geometries of four Camellia sinensis phytochemicals, Cyanidin, Epicatechin, Malvidin, and Petunidin, were investigated via DFT calculation to explore their structural parameters and intrinsic dipole moments. As visualized in Figure 6, each molecule reveals a distinct spatial arrangement and orientation of its dipole moment, quantified in Debye units. Cyanidin exhibits a moderately high dipole moment of 5.408 D, while Epicatechin shows the lowest value at 2.706 D, indicating a more symmetrical electron distribution (Ortix, 2021). In contrast, Malvidin and Petunidin possess higher dipole moments of 7.846 D and 7.399 D, respectively, suggesting a more polar character, which may influence their interaction profiles with biomolecular targets, particularly in polar environments such as the active site of enzymes or aqueous biological systems (Jorge *et al*., 2022). The bond length parameters for C–O, O–H, C–C, C=C, and C–H in each compound, presented in Table 5, further validate the optimized geometries. Cyanidin, Malvidin, and Petunidin exhibit nearly identical C–O and O–H bond lengths (~1.327–1.328 Å and 0.960 Å, respectively), indicative of their shared anthocyanidin backbone (Szewczuk *et al*., 2023). Epicatechin, differing structurally as a flavanol, exhibits a slightly longer C–O bond (1.423 Å) and a marginally shorter O–H bond (0.958 Å), reflecting its unique ring configuration and functional group placement (Eugène *et al*., 2022). The consistent C=C bond lengths across all molecules (~1.374–

1.385 Å) confirm the retention of aromaticity in the phenyl rings, while minor variations in C–C and C–H bonds are within acceptable theoretical limits and are influenced by conjugation and steric effects (Jin *et al*., 2022). These results confirm that all four compounds adopt stable geometries suitable for subsequent quantum chemical analysis, molecular docking, and ADME predictions relevant to neurodegenerative targets in Parkinson's disease.

Table 5: Selected Bond Lengths (in Å) obtained from DFT-Optimized Geometries of Camellia Sinensis Phytochemicals Structural Features are Compared across Five Common Bond Types: C–O, O–H, C–C, C=C, and C–H

Compounds	C-O (Å)	O-H (Å)	C-C (Å)	C=C (Å)	C-H (Å)
Cyanidin	1.327	0.960	1.412	1.374	1.084
Epicatechin	1.423	0.958	1.530	1.381	1.100
Malvidin	1.328	0.960	1.417	1.385	1.079
Petunidin	1.327	0.960	1.415	1.376	1.079

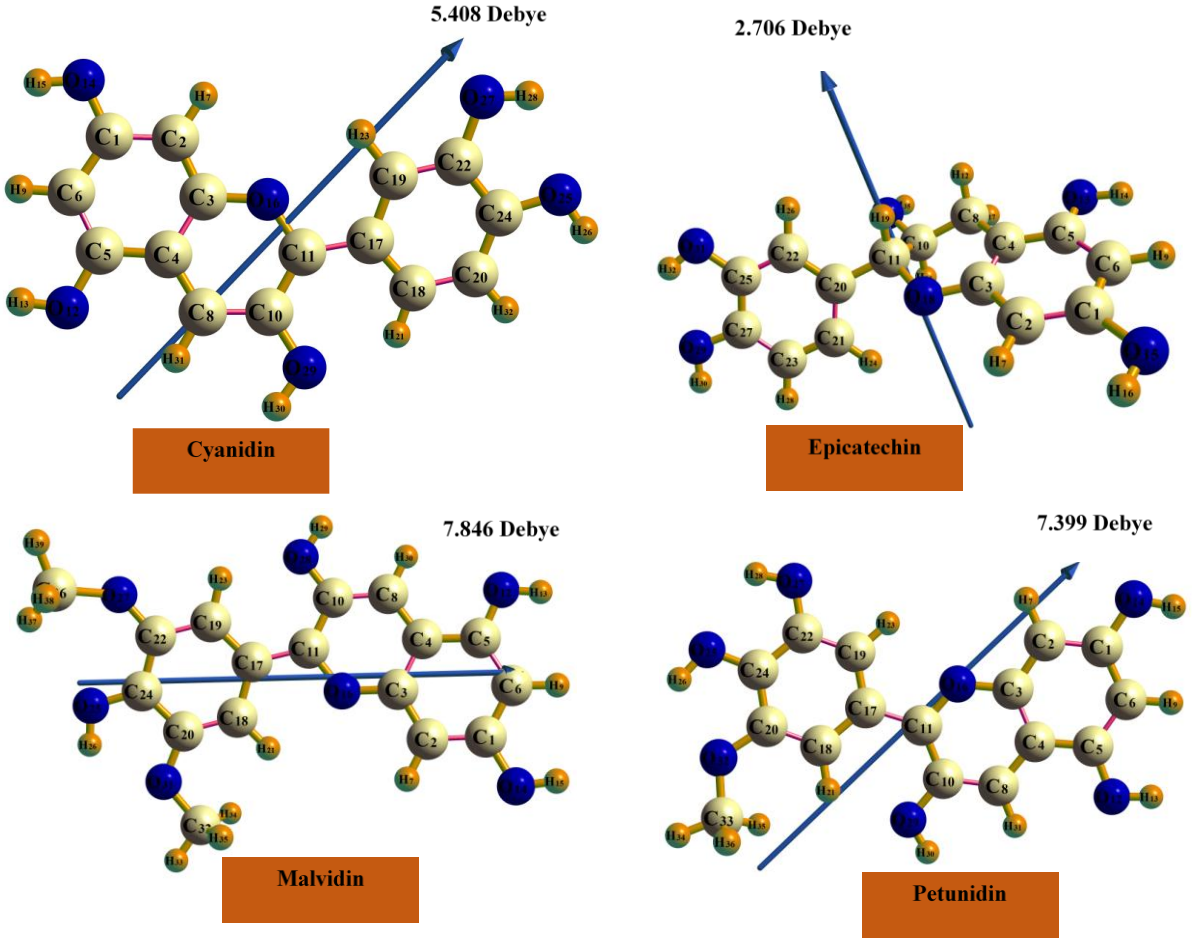

Figure 6: Optimized Molecular Geometries and Dipole Moment Vectors (Debye) of four Camellia Sinensis Phytochemicals, Cyanidin, Epicatechin, Malvidin, and Petunidin, Computed using DFT. The Arrow Indicates the Direction and Magnitude of the Dipole Moment in Each Molecule

Quantum Chemical Descriptors

Frontier molecular orbital analysis provides crucial insight into the electronic distribution, reactivity, and stability of bioactive molecules. The highest occupied molecular orbitals (HOMO) and lowest unoccupied molecular orbitals (LUMO) for Cyanidin, Epicatechin, Malvidin, and Petunidin are illustrated in Figure 7. The spatial distribution of these orbitals shows that HOMOs are largely localized over the conjugated aromatic rings and hydroxyl substituents, indicating potential electron-donating sites. In contrast, the LUMOs are spread over similar conjugated frameworks, designating possible sites for electrophilic attack.

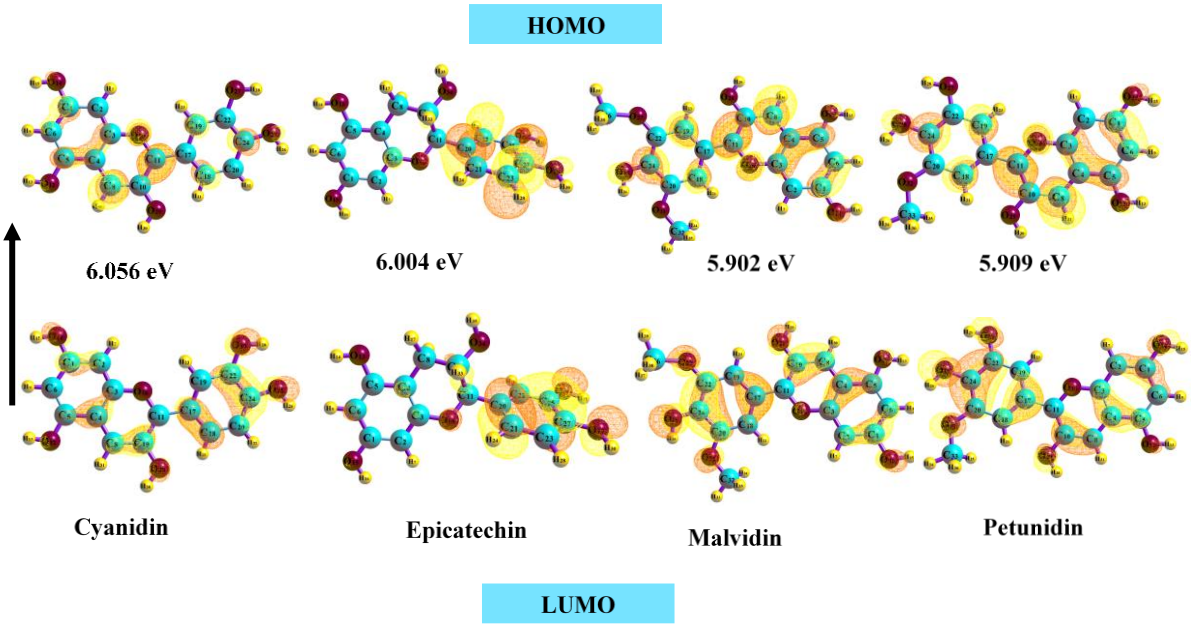

Figure 7: HOMO and LUMO Contour Plots of Cyanidin, Epicatechin, Malvidin, and Petunidin. Corresponding HOMO–LUMO Energy Gaps (in eV) are Indicated below Each Compound. The Colored Lobes Represent the Spatial Distribution of Electron Densities in Frontier Orbitals

The electron density localization in both HOMO and LUMO suggests that these molecules can undergo π–π stacking and hydrogen bonding interactions, crucial for binding with neurodegenerative targets in Parkinson's disease. The HOMO–LUMO energy gap (ΔE) is a critical indicator of kinetic stability and molecular reactivity (Glendening *et al*., 2019). Among the studied compounds, Malvidin (ΔE = 5.902 eV) and Petunidin (ΔE = 5.909 eV) possess the lowest gaps, suggesting higher electronic softness and potential biological reactivity. Cyanidin (ΔE = 6.056 eV) exhibits the largest gap, implying greater stability but slightly reduced reactivity under physiological conditions. Epicatechin's ΔE (6.004 eV) is comparable to Cyanidin's, but it is much higher E_{LUMO} (–1.775 eV) and lower E_{HOMO} (–7.779 eV) signify less pronounced electron-accepting and -donating capacities. Quantum chemical descriptors derived from HOMO and LUMO values further reinforce these observations (Table 6). Electronegativity (χ) and chemical potential (μ) are highest in Cyanidin and Petunidin, highlighting their greater tendency to attract electrons (Zhan *et al*., 2003; Badeji *et al*., 2024). The global hardness (η) values reflect the compounds' resistance to electronic deformation (Franco-Pérez *et al*., 2018), with Cyanidin again emerging as the most chemically hard compound (η = 3.028 eV). Conversely, Petunidin and Malvidin possess slightly lower η values (2.954 and 2.951 eV), indicating increased polarizability and responsiveness to interactions. The electrophilicity index (ω), a predictor of biological affinity and molecular toxicity (Pal & Chattaraj, 2023), is highest for Cyanidin (10.266 eV), followed closely by Petunidin (10.203 eV) and Malvidin (10.077 eV). Epicatechin has a significantly lower ω value (3.801 eV), which aligns with its lower dipole moment and weaker polarization properties. The softness parameter (σ), which inversely relates to hardness (Pearson, 2005), follows a similar trend and highlights the readiness of Malvidin and Petunidin to participate in electron exchange processes. In conclusion, these results suggest that Malvidin and Petunidin are the most chemically reactive and polarizable candidates, rendering them promising scaffolds for further exploration as neuroprotective agents through enhanced electronic and pharmacological interactions.

Table 6: Quantum Chemical Descriptors of Selected *Camellia Sinensis* Phytochemicals Computed from LUMO and HOMO Energy Values. Ionization Potential = IP, Electron Affinity = EA, Global Hardness = η, Global Softness = σ, Chemical Potential = μ, Electronegativity = χ, Electrophilicity Index = ω

Parameter	E_{LUMO} (eV)	E_{HOMO} (eV)	ΔE (eV)	EA (eV)	IP (eV)	Ƞ (eV)	σ (eV^{-1})	μ (eV)	χ (eV)	ω (eV)
Cyanidin	-4.857	-10.913	6.056	4.857	10.913	3.028	1.514	-7.885	7.885	10.266
Epicatechin	-1.775	-7.779	6.004	1.775	7.779	3.002	1.501	-4.777	4.777	3.801
Malvidin	-4.761	-10.663	5.902	4.761	10.663	2.951	1.476	-7.712	7.712	10.077
Petunidin	-4.809	-10.718	5.909	4.809	10.718	2.954	1.477	-7.764	7.764	10.203

Natural Bond Order (NBO) Analysis

NBO analysis was employed to provide insight into the intramolecular electron delocalization and donor–acceptor interactions that contribute to the stability and reactivity of *Camellia sinensis* phytochemicals. The Fock matrix elements (F(i,j)), second-order perturbation energy (E^2), and the energy gap between donor and acceptor orbitals (E(j)–E(i)), were calculated to quantify the strength of these interactions (Table 7). Among all interactions, the most significant stabilization energy was observed in both Malvidin and Petunidin, where lone pair donation from oxygen atom O16 (LP(2) O_{16}) to the antibonding orbital of carbon C11 (LP*(1) C11) exhibited exceptionally high E^2 values of 138.56 kcal/mol and 138.76 kcal/mol, respectively. This strong intramolecular charge transfer highlights the crucial role of oxygen lone pair interactions in enhancing electronic delocalization and

molecular stability (Halim *et al*., 2024). The high F(i,j) values (0.203) and moderate energy gaps (0.30 eV) support the efficient donor–acceptor overlap and coupling strength (Golding Sheeba *et al*., 2021). In Cyanidin, notable delocalization occurs from π orbitals of C_{17}–C_{18} and C_8–C_{10} into the antibonding LP*(1) orbital of C_{11}, contributing 83.72 kcal/mol and 51.95 kcal/mol stabilization, respectively. These interactions underline the importance of conjugated π systems in stabilizing the molecule through hyperconjugation. Epicatechin, lacking extensive conjugation compared to anthocyanidins, exhibits lower stabilization energies. The π→π* delocalization between adjacent aromatic bonds (C_2–C_3 to C_1–C_6 and C_4–C_5 to C_2–C_3) contributes E^2 values of 41.51 and 39.36 kcal/mol, respectively, reflecting moderate resonance stabilization within its aromatic ring system. These donor–acceptor interactions collectively influence the electronic distribution and chemical reactivity of the molecules, especially in binding environments, where such delocalization effects can play a vital role in stabilizing ligand–target complexes (Sin *et al*., 2022). The enhanced delocalization seen in Malvidin and Petunidin further supports their potential as reactive and biologically significant species for therapeutic applications in Parkinson's disease.

Table 7: Second-Order Perturbation Energies (e^2), Energy Differences [e(j)–e(i)], and Fock Matrix Elements [f(i,j)] of Key Donor–Acceptor Interactions Derived from Nbo Analysis of Camellia Sinensis Phytochemicals. Strong Delocalizations Indicate Enhanced Intramolecular Stabilization

Compounds	Donor (i)	Acceptor (j)	$E^{(2)}$ kcal/mol	E(j)-E(i)	F(I,j)
Cyanidin	π C_{17} - C_{18}	LP*(1) C_{11}	83.72	0.15	0.110
	π C_8 - C_{10}	LP*(1)C_{11}	51.95	0.22	0.111
Epicatechin	π C_2 - C_3	π^* C_1 - C_6	41.51	0.37	0.112
	π C_4 - C_5	π^*C_2 - C_3	39.36	0.38	0.110
Malvidin	LP (2) O_{16}	LP*(1) C_{11}	138.56	0.30	0.203
	π C_{19} - C_{22}	LP*(1) C_{24}	93.29	0.17	0.136
Petunidin	LP (2) O_{16}	LP*(1) C_{11}	138.76	0.30	0.203
	π C_{17} - C_{18}	LP*(1) C_{11}	80.42	0.15	0.109

Molecular Electrostatic Potential Analysis (MEP)

The MEP maps provide a three-dimensional representation of the charge distribution on molecular surfaces, offering insight into potential sites for nucleophilic and electrophilic attack. In Figure 8, MEP surfaces of Cyanidin, Epicatechin, Malvidin, and Petunidin reveal areas of negative and positive electrostatic potential, illustrated by red (electron-rich), blue (electron-deficient), and green (neutral) zones (Suresh *et al*., 2022; Pal & Chattaraj, 2023). Across all compounds, intense red regions are prominently located near oxygen atoms of hydroxyl groups, signifying strong nucleophilic character and the potential to form hydrogen bonds or coordinate with electrophilic residues in biological targets. The blue regions, although less widespread, mark the electrophilic centers susceptible to nucleophilic attack. These features reflect the molecules' capacity for interaction with active sites in biomacromolecules such as enzymes and receptors involved in neurodegeneration. Notably, the MEP maps correspond well with the computed electrophilicity indices (ω) derived from FMO analysis. Cyanidin, Malvidin, and Petunidin exhibit high ω values (10.266 eV, 10.077 eV, and 10.203 eV, respectively), and their MEP maps display well-defined positive (blue) zones indicating strong electron-accepting capacity. This high electrophilicity is consistent with their observed capability to stabilize excess electronic charge, which is particularly important in biological systems where electrophilic ligands interact with nucleophilic amino acid residues. Epicatechin, in contrast, shows a lower electrophilicity index (ω = 3.801 eV) and its MEP surface appears more diffuse and less polarized, with broader green areas indicating a more even charge distribution and reduced electrophilic reactivity. This suggests that while Epicatechin may still engage in biological interactions, its potential as an electrophilic species is relatively limited compared to the anthocyanidin derivatives. Thus, the correlation between MEP visualization and electrophilicity indices provides a comprehensive view of the electronic behavior of these phytochemicals. These characteristics support the hypothesis that Cyanidin, Malvidin, and Petunidin may serve as more reactive and selective ligands in the modulation of protein targets associated with Parkinson's disease pathology.

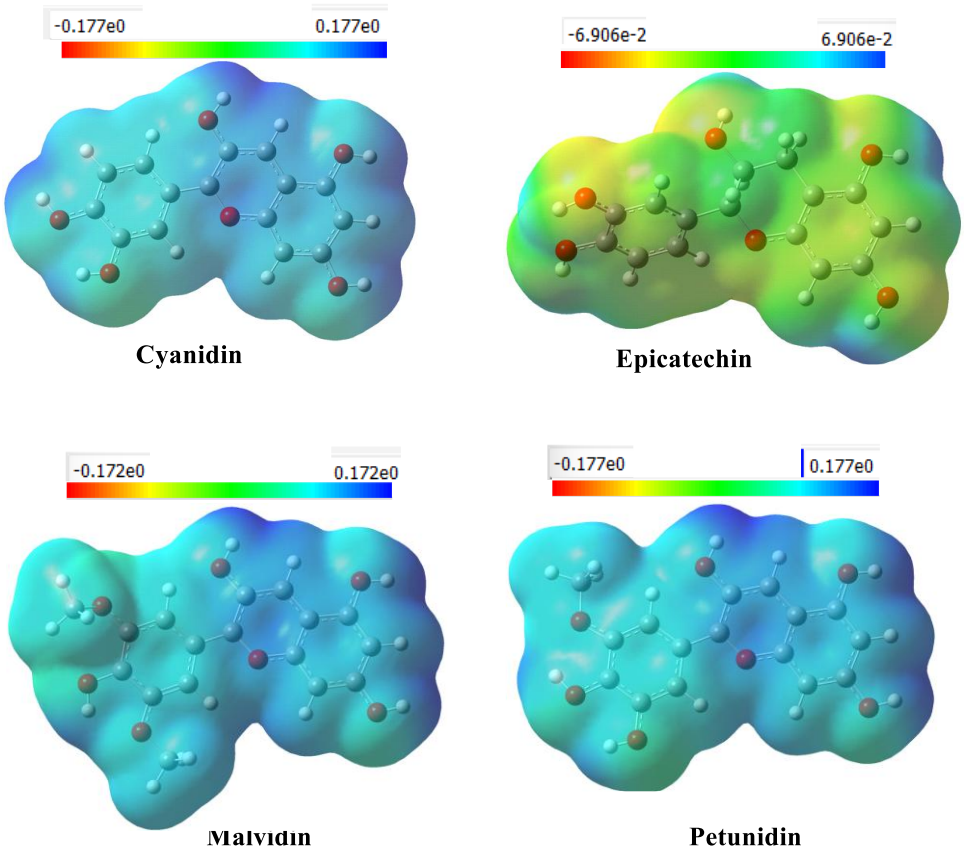

Figure 8: Molecular Electrostatic Potential (MEP) Surfaces of Cyanidin, Epicatechin, Malvidin, and Petunidin. Red Regions Indicate Electron-rich (Nucleophilic) Sites, Blue Indicates Electron-deficient (Electrophilic) Sites, and green Represents Neutral Potential. These MEP Patterns Correspond to Electrophilicity Indices Obtained from FMO Calculations

Relationship between Physicochemical Properties, Quantum Chemical Descriptors, Inhibitory Potential, and Pharmacokinetics of *Camellia Sinensis* Phytochemicals

The inhibitory potential and pharmacokinetic behavior of *Camellia sinensis* phytochemicals are closely governed by their physicochemical and electronic properties, as revealed by DFT calculations. The quantum chemical descriptors derived from DFT studies elucidate how the chemical structure correlates with biological activity and drug-likeness. The FMO for cyanidin, malvidin, and petunidin showed that HOMO densities were fully delocalized around the hydroxyl-substituted region on the aromatic systems, suggesting that they are electron donors, capable of engaging in hydrogen bonding and participate in π–π stacking with targets in neurodegenerative diseases such as LRRK2, A2AR, and MAO-B. LUMO distributions were mainly localized around the conjugated aromatic systems, which provided specific sites for their electrophilic centres for nucleophilic protein residues. The ΔE values were least for malvidin (5.902 eV) and petunidin (5.909 eV), indicating softness and high reactivity, consistent with their superior inhibitive potential against MAO-B and LRRK2. The ΔE value of epicatechin (6.004 eV) on the other hand, was higher than the others and also have relatively low electrophilicity index (3.801 eV), which contributed to its low reactivity and weaker inhibition compared to malvidin and petunidin.

Natural bond orbital (NBO) analysis also confirmed that petunidin and malvidin exhibited the strongest intramolecular charge delocalization, with a stabilization energy of above 138 kcal/mol from oxygen lone pair donating into antibonding orbitals. This enhanced electronic delocalization explains their improved binding free energies (for petunidin with MAO-B = –44.49 kcal/mol, and with LRRK2 = –38.48 kcal/mol), surpassing that of the reference drugs: rasagiline and DNL201. In support of this findings, the MEP maps showed the high electron density areas (red), as centered around the hydroxyl groups, would allow for nucleophilic reaction with the protein residues. The three compounds cyanidin, malvidin, and petunidin exhibited fully polarised surfaces, indicative of strong electrophilicity, confirming their suitability for selective ligand-target interactions.

All of the phytochemicals studied followed Lipinski's Rule of Five allowing for high gastro-intestinal absorption, an important consideration for establishing oral bioavailability. Also as one would expect, the additional dipole moments (malvidin, 7.846 D; petunidin, 7.399 D.) allow for greater solubility within the polar bio-environments for interactions for the neuroprotective agents, also consistent with the higher stability from the MD simulations. The comparatively weak dipole moment of epicatechin (2.706 D) and the dispersive nature of the MEP surface could be responsible for its weaker interaction profile and reduced pharmacological potency. These findings reveal that DFT studies results directly correlate with the inhibitory potential observed in the MD simulations and also the dipole moment is in agreement with drug-likeness rules, ensuring favorable pharmacokinetics. Therefore the findings identify cyanidin, malvidin and petunidin as lead candidates with optimal balance between reactivity, inhibitory strength, and pharmacokinetic feasibility for neurodegenerative disease therapy.

CONCLUSION

This study presents an integrated computational evaluation of Camellia sinensis phytochemicals as multi-target neuroprotective candidates against Parkinson's disease, combining molecular docking, 100 ns molecular dynamics simulations, MM/PBSA binding free energy calculations, density functional theory (DFT) analysis, pharmacokinetic profiling, and in silico toxicity prediction.

Thermodynamic binding free energy analysis revealed that several phytochemicals exhibit competitive or superior binding compared to reference drugs. In the LRRK2 system, Petunidin demonstrated the most favorable binding free energy (ΔG_bind = −38.48 ± 3.96 kcal/mol), outperforming the reference inhibitor DNL-201 (−27.31 ± 2.18 kcal/mol), while Cyanidin also showed strong affinity (−31.96 ± 3.51 kcal/mol). For A2AR, Epigallocatechin (−36.43 ± 3.58 kcal/mol) displayed substantial binding stability relative to Istradefylline (−49.71 ± 3.45 kcal/mol). In the MAO-B system, Petunidin (−44.50 kcal/mol) and Malvidin (−41.49 ± 3.29 kcal/mol) exhibited stronger binding than the reference drug Rasagiline (−33.51 ± 2.40 kcal/mol). These findings highlight Petunidin and Cyanidin as promising dual-target inhibitors across multiple Parkinson's disease-associated proteins.

Molecular dynamics analyses further confirmed structural stability. LRRK2–Petunidin complexes exhibited the lowest RMSD (3.369 ± 0.564 Å) among the phytochemical-bound systems, indicating enhanced structural stabilization relative to the APO form. Similar stability trends were observed in A2AR and MAO-B complexes, where ligand-bound systems maintained comparable or improved RMSD and radius of gyration values relative to controls. Although localized fluctuations (RMSF) were observed in flexible loop regions, the overall compactness and conformational integrity of the complexes were preserved throughout the 100 ns simulations. DFT calculations provided mechanistic insight into the electronic determinants of inhibitory activity. Malvidin and Petunidin exhibited relatively small HOMO–LUMO energy gaps (~5.90 eV), indicating higher chemical softness and reactivity in biological environments. Cyanidin displayed the highest electrophilicity index (10.266 eV), consistent with its strong electrostatic interaction contributions observed in MM/PBSA analysis. NBO analysis revealed significant intramolecular charge delocalization in Malvidin and Petunidin, enhancing molecular stability, while molecular electrostatic potential (MEP) mapping identified electron-rich hydroxyl regions that facilitate hydrogen bonding and π–π stacking interactions within the active sites of LRRK2, A2AR, and MAO-B.

Pharmacokinetic evaluation demonstrated that all selected phytochemicals comply with Lipinski's Rule of Five, with favorable molecular weights (<500 Da), acceptable lipophilicity (LogP <5), TPSA ≤140 Å², and high predicted gastrointestinal absorption. However, limited blood–brain barrier permeability suggests that structural optimization or advanced delivery strategies may be required to enhance central nervous system availability. Toxicity prediction using ProTox 3.0 indicated generally acceptable safety margins, with high predicted LD_{50} values for most compounds and no predicted hepatotoxicity. Neurotoxicity alerts were observed only for methylxanthines (caffeine and theobromine), while carcinogenicity predictions were limited to specific anthocyanidins, warranting further experimental validation.

Therefore, this multi-level computational investigation identifies Petunidin, Cyanidin, and Malvidin as promising multi-target scaffolds with favorable binding energetics, structural stability, electronic reactivity, and acceptable drug-like properties. Future studies should focus on structural optimization to improve BBB permeability, experimental validation through in vitro enzyme inhibition and neuronal cell models, and in vivo pharmacodynamic and safety assessment. The translational potential of this work lies in advancing plant-derived, multi-target therapeutic candidates for Parkinson's disease drug development.

REFERENCES

Adegbesan, B. O., Ezima, E. N., Hassan, B. O., Kehinde, J. O., Adewale, A. A., Osonuga, I. O., Olalekan, S. O. (2024). Evaluation of in vitro antioxidant activities, total phenolic and elemental contents of common herbs and spices (Moringa oleifera leaves, Allium sativum (Garlic) and Momordica charantia (ejinrin) leaves) in South-West Nigeria. Pure and Applied Chemistry, 96 (10), 1339–1349. https://doi.org/10.1515/pac-2023-1128

Adeyanju, M. M., Saheed, I. A., Oyelekan, O. I., Dele-Osibanjo, T. A., Adelegan, A. A., Raimi, A. J., Olalekan, S. O., Alabi, O. S., & Alli, K. M. (2022). Sesamum indicum diet prevents hyperlipidemia in experimental rats. Food Chemistry: Molecular Sciences, 4, 100092.

Andrienko, G. (2010). Chemcraft-graphical software for visualization of quantum chemistry computations. See Https://Www.Chemcraftprog.Com.

Atanasov, A. G., Zotchev, S. B., Dirsch, V. M., the International Natural Product Sciences Taskforce, Orhan, I. E., Banach, M., Rollinger, J. M., Barreca, D., Weckwerth, W., Bauer, R., Bayer, E. A., Majeed, M., Bishayee, A., Bochkov, V., Bonn, G. K., Braidy, N., Bucar, F., Cifuentes, A., D'Onofrio, G., … Supuran, C. T. (2021). Natural products in drug discovery: Advances and opportunities. Nature Reviews Drug Discovery, 20(3), 200–216. https://doi.org/10.1038/s41573-020-00114-z

Badeji, A. A., Omoniyi, M. T., Ogunbayo, T. B., Oladipo, S. D., & Akinbulu, I. A. (2024). Quantum chemical investigation of the degradation of acid orange 7 by different oxidants. Discover Chemistry, 1(1), 55. https://doi.org/10.1007/s44371-024-00059-x

Badeji, A. A., Olalekan, S. O., Oladipo, S. D., Obakachi, V. A., Osinubi, A. D., Familoni, O., Asekun, O. T., & Anselm, O. H. (2025). Anti-diabetic potentials of L-prolinamides: A computational study. Discover Chemistry, 2(1), 209. https://doi.org/10.1007/s44371-025-00281-1

Bogetofte, H., Alamyar, A., Blaabjerg, M., & Meyer, M. (2020). Levodopa therapy for Parkinson's disease: History, current status and perspectives. CNS & Neurological Disorders-Drug Targets-CNS & Neurological Disorders), 19(8), 572–583.

Cenci, M. A., Skovgård, K., & Odin, P. (2022). Non-dopaminergic approaches to the treatment of motor complications in Parkinson's disease. Neuropharmacology, 210, 109027. https://doi.org/10.1016/j.neuropharm.2022.109027

Dahlin, J. L., Nissink, J. W. M., Strasser, J. M., Francis, S., Higgins, L., Zhou, H., Zhang, Z., & Walters, M. A. (2015). PAINS in the Assay: Chemical Mechanisms of Assay Interference and Promiscuous Enzymatic Inhibition Observed during a Sulfhydryl-Scavenging HTS. Journal of Medicinal

Chemistry, 58(5), 2091–2113. https://doi.org/10.1021/jm5019093

Daina, A., Michielin, O., & Zoete, V. (2017). SwissADME: A free web tool to evaluate pharmacokinetics, drug-likeness and medicinal chemistry friendliness of small molecules. Scientific Reports, 7, 42717. https://doi.org/10.1038/srep42717

Datta, D., Shee, N. K., & Von Szentpály, L. (2013). Chemical Potential of Molecules Contrasted to Averaged Atomic Electronegativities: Alarming Differences and Their Theoretical Rationalization. The Journal of Physical Chemistry A, 117(1), 200–206. https://doi.org/10.1021/jp3103386

De Colibus, L., Li, M., Binda, C., Lustig, A., Edmondson, D. E., & Mattevi, A. (2005). Three-dimensional structure of human monoamine oxidase A (MAO A): Relation to the structures of rat MAO A and human MAO B. Proceedings of the National Academy of Sciences of the United States of America, 102(36), 12684–12689. https://doi.org/10.1073/pnas.0505975102

Dennington, R., Keith, T., & Millam, J. (2023). GaussView, Version 6.0. 1.6, Semichem Inc., Shawnee Mission, KS, 2016. There Is No Corresponding Record for This Reference.

Durrant, J. D., & McCammon, J. A. (2011). Molecular dynamics simulations and drug discovery. BMC Biology, 9(1), 71. https://doi.org/10.1186/1741-7007-9-71

Ekoro, I. A., & Odeja, O. O. (2026). Molecular docking and theoretical toxicity assessment of bioactive constituents of leaf and root bark essential oils from Spondia dulcis. FUDMA JOURNAL OF SCIENCES, 10(3). https://doi.org/10.33003/fjs-2026-1003-4601

Eugène, E. A., Robert, N. B., Ganiyou, A., Denis, Y. K., Ané, A., & Sawaliho, B. E. H. (2022). Catechin and Epicatechin. What's the More Reactive? Computational Chemistry, 10(02), 53–70. https://doi.org/10.4236/cc.2022.102003

Finberg, J. P. M. (2010). Pharmacology of Rasagiline, a New MAO-B Inhibitor Drug for the Treatment of Parkinson's Disease with Neuroprotective Potential. Rambam Maimonides Medical Journal, 1(1), e0003. https://doi.org/10.5041/RMMJ.10003

Franco-Pérez, M., Polanco-Ramírez, C. A., Gázquez, J. L., & Ayers, P. W. (2018). Local and nonlocal counterparts of global descriptors: The cases of chemical softness and hardness. Journal of Molecular Modeling, 24(10), 285. https://doi.org/10.1007/s00894-018-3823-4

Friesner, R. A., Banks, J. L., Murphy, R. B., Halgren, T. A., Klicic, J. J., Mainz, D. T., Repasky, M. P., Knoll, E. H., Shelley, M., Perry, J. K., Shaw, D. E., Francis, P., & Shenkin, P. S. (2004). Glide: A New Approach for Rapid, Accurate Docking and Scoring. 1. Method and Assessment of Docking Accuracy. Journal of Medicinal Chemistry, 47(7), 1739–1749. https://doi.org/10.1021/jm0306430

Frisch, M., Trucks, G., Schlegel, H., Scuseria, G., Robb, M., Cheeseman, J., Scalmani, G., Barone, V., Petersson, G., & Nakatsuji, H. (2016). Gaussian 16 Revision C. 01, 2016. Gaussian Inc. Wallingford CT, 1, 572.

Gahtani, R. M., Shoaib, S., Hani, U., Jayachithra, R., Alomary, M. N., Chauhan, W., Jahan, R., Tufail, S., & Ansari, M. A. (2024). Combating Parkinson's disease with plant-derived polyphenols: Targeting oxidative stress and neuroinflammation. Neurochemistry International, 178, 105798. https://doi.org/10.1016/j.neuint.2024.105798

Glendening, E. D., Landis, C. R., & Weinhold, F. (2019). NBO 7.0: New vistas in localized and delocalized chemical bonding theory. Journal of Computational Chemistry, 40(25), 2234–2241. https://doi.org/10.1002/jcc.25873

Golding Sheeba, G., Usha, D., Amalanathan, M., Sony Michael Mary, M., & MarshanRobert, H. (2021). Molecular structure, vibrational spectroscopic, frontier molecular orbital and natural bond orbital analysis of anti-cancer drug 6-chloro-3- pyridine carbonitrile. Spectroscopy Letters, 54(6), 419–436. https://doi.org/10.1080/00387010.2021.1932964

Goyal, R., Mittal, P., Gautam, R. K., Kamal, M. A., Perveen, A., Garg, V., Alexiou, A., Saboor, M., Haque, S., & Farhana, A. (2024). Natural products in the management of neurodegenerative diseases. Nutrition & Metabolism, 21(1), 26.

Halim, S. A., El-Meligy, A. B., El-Nahas, A. M., & El-Demerdash, S. H. (2024). DFT study, and natural bond orbital (NBO) population analysis of 2-(2-Hydroxyphenyl)-1-azaazulene tautomers and their mercapto analouges. Scientific Reports, 14(1), 219. https://doi.org/10.1038/s41598-023-50660-w

Herraiz, T., & Guillén, H. (2018). Monoamine Oxidase-A Inhibition and Associated Antioxidant Activity in Plant Extracts with Potential Antidepressant Actions. BioMed Research International, 2018, 1–10. https://doi.org/10.1155/2018/4810394

Ho, P. W.-L., Chang, E. E.-S., Leung, C.-T., Liu, H., Malki, Y., Pang, S. Y.-Y., Choi, Z. Y.-K., Liang, Y., Lai, W. S., Ruan, Y., Leung, K. M.-Y., Yung, S., Mak, J. C.-W., Kung, M. H.-W., Ramsden, D. B., & Ho, S.-L. (2022). Long-term inhibition of mutant LRRK2 hyper-kinase activity reduced mouse brain α-synuclein oligomers without adverse effects. Npj Parkinson's Disease, 8(1), 1–22. https://doi.org/10.1038/s41531-022-00386-9

Houk, K. N. (1977). Applications of Frontier Molecular Orbital Theory to Pericyclic Reactions. In Organic Chemistry: A Series of Monographs (Vol. 35, pp. 181–271). Elsevier. https://doi.org/10.1016/B978-0-12-470502-9.50010-9

Huang, Y., Rong, C., Zhang, R., & Liu, S. (2017). Evaluating frontier orbital energy and HOMO/LUMO gap with descriptors from density functional reactivity theory. Journal of Molecular Modeling, 23(1), 3. https://doi.org/10.1007/s00894-016-3175-x

Jacobson, M. P., Pincus, D. L., Rapp, C. S., Day, T. J. F., Honig, B., Shaw, D. E., & Friesner, R. A. (2004). A hierarchical approach to all ‐ atom protein loop prediction. Proteins: Structure, Function, and Bioinformatics, 55(2), 351 ‐ 367. https://doi.org/10.1002/prot.10613

Jennings, D., Huntwork-Rodriguez, S., Henry, A. G., Sasaki, J. C., Meisner, R., Diaz, D., Solanoy, H., Wang, X., Negrou, E., Bondar, V. V., Ghosh, R., Maloney, M. T., Propson, N. E.,

Zhu, Y., Maciuca, R. D., Harris, L., Kay, A., LeWitt, P., King, T. A., … Troyer, M. D. (2022). Preclinical and clinical evaluation of the LRRK2 inhibitor DNL201 for Parkinson's disease. Science Translational Medicine, 14(648), eabj2658. https://doi.org/10.1126/scitranslmed.abj2658

Jin, X., Li, S., Guo, L., Hua, J., Qu, D.-H., Su, J., Zhang, Z., & Tian, H. (2022). Interplay of Steric Effects and Aromaticity Reversals to Expand the Structural/Electronic Responses of Dihydrophenazines. Journal of the American Chemical Society, 144(11), 4883–4896. https://doi.org/10.1021/jacs.1c12610

Jinsmaa, Y., Florang, V. R., Rees, J. N., Mexas, L. M., Eckert, L. L., Allen, E. M., Anderson, D. G., & Doorn, J. A. (2011). Dopamine-derived biological reactive intermediates and protein modifications: Implications for Parkinson's disease. Chemico-Biological Interactions, 192(1–2), 118–121. https://www.sciencedirect.com/science/article/pii/S0009279711000111

Jorge, M., Gomes, J. R. B., & Barrera, M. C. (2022). The dipole moment of alcohols in the liquid phase and in solution. Journal of Molecular Liquids, 356, 119033. https://doi.org/10.1016/j.molliq.2022.119033

Koeglsperger, T., Rumpf, S.-L., Schließer, P., Struebing, F. L., Brendel, M., Levin, J., Trenkwalder, C., Höglinger, G. U., & Herms, J. (2023). Neuropathology of incidental Lewy body & prodromal Parkinson's disease. Molecular Neurodegeneration, 18(1), 32.

Kotaru, S., Pokhilko, P., & Krylov, A. I. (2022). Spin–orbit couplings within spin-conserving and spin-flipping time-dependent density functional theory: Implementation and benchmark calculations. The Journal of Chemical Physics, 157(22), 224110. https://doi.org/10.1063/5.0130868

Krishnakumar, H., Jayaraman, M., Prabhu, D., & Jeyakanthan, J. (2026). Structure-guided discovery of marine natural products as glucokinase activators for type 2 diabetes mellitus: A computational perspective. Journal of Molecular Graphics and Modelling, 142, 109181. https://doi.org/10.1016/j.jmgm.2025.109181

Kuzemsky, A. L. (2015). Variational principle of Bogoliubov and generalized mean fields in many-particle interacting systems. International Journal of Modern Physics B, 29(18), 1530010. https://doi.org/10.1142/S0217979215300108

Li, C., Lin, J., Yang, T., & Shang, H. (2022). Green Tea Intake and Parkinson's Disease Progression: A Mendelian Randomization Study. Frontiers in Nutrition, 9, 848223. https://doi.org/10.3389/fnut.2022.848223

Li, J. W.-H., & Vederas, J. C. (2009). Drug Discovery and Natural Products: End of an Era or an Endless Frontier? Science, 325(5937), 161–165. https://doi.org/10.1126/science.1168243

Loncharich, R. J., Brooks, B. R., & Pastor, R. W. (1992). Langevin dynamics of peptides: The frictional dependence of isomerization rates of N-acetylalanyl-N'-methylamide—PubMed. https://doi.org/10.1002/bip.360320508

Malar, D. S., Prasanth, M. I., Brimson, J. M., Sharika, R., Sivamaruthi, B. S., Chaiyasut, C., & Tencomnao, T. (2020a). Neuroprotective Properties of Green Tea (Camellia sinensis) in Parkinson's Disease: A Review. Molecules, 25(17), 3926. https://doi.org/10.3390/molecules25173926

Mishal, B., Shetty, A., & Wadia, P. (2023). Adverse effects of medications used to treat motor symptoms of Parkinson's disease: A narrative review. Annals of Movement Disorders, 6(2), 45. https://doi.org/10.4103/aomd.aomd_37_22

Mohd Sairazi, N. S., & Sirajudeen, K. (2020). Natural products and their bioactive compounds: Neuroprotective potentials against neurodegenerative diseases. Evidence‐Based Complementary and Alternative Medicine, 2020(1), 6565396.

Nair, P. C., & Miners, J. O. (2014). Molecular dynamics simulations: From structure function relationships to drug discovery. In Silico Pharmacology, 2(1), 4. https://doi.org/10.1186/s40203-014-0004-8

Obakachi, V. A., Kehinde, I., Kushwaha, N. D., Akinpelu, O. I., Kushwaha, B., Merugu, S. R., Kayamba, F., Kumalo, H. M., & Karpoormath, R. (2022). Structural based investigation of novel pyrazole-thiazole Hybrids as dual CDK-1 and CDK-2 inhibitors for cancer chemotherapy. Molecular Simulation, 48(8), 687–701.

Ohno, Y., Suzuki, M., Asada, H., Kanda, T., Saki, M., Miyagi, H., Yasunaga, M., Suno, C., Iwata, S., & Saito, J. (2023). In vitro pharmacological profile of KW-6356, a novel adenosine A2A receptor antagonist/inverse agonist. Molecular Pharmacology, 103(6), 311–324. https://www.sciencedirect.com/science/article/pii/S0026895X24012823

Okwute, P. G., Oluwatunase, G. O., Mofolorunso, A. M., Asafa, O. O., Ogunbiyi, O. E., & Olalekan, S. (2023a). Evaluation of Abrus precatorius on reproductive function of male Wistar rat. Anatomy Journal of Africa, 12(2), 2384–2392.

Okwute, P. G., Oluwatunase, G. O., Mofolorunso, A. M., Asafa, O. O., Ogunbiyi, O. E., & Olalekan, S. (2023b). Evaluation of Abrus precatorius on reproductive function of male Wistar rat. Anatomy Journal of Africa, 12(2), 2384–2392. https://www.ajol.info/index.php/aja/article/view/253035

Oladipo, S., Adeleke, A. A., Badeji, A. A., Babalola, K. I., Labulo, A. H., Hassan, I., Yussuf, S. T., & Olalekan, S. O. (2024). Computational investigation and biological activity of selected Schiff bases. Journal of the Nigerian Society of Physical Sciences, 2103–2103. https://doi.org/10.46481/jnsps.2024.2103

Oladipo, S. D., Luckay, R. C., Badeji, A. A., Zamisa, S. Z., Olalekan, S. O., & Oladoye, P. O. (2025a). Structural studies, DFT computational analysis and inhibitory potential of (E)-N'-(2-bromophenyl)-N-(2,6-diisopropylphenyl)formamidine against CDK1 and CDK2. Journal of Molecular Structure, 1320, 139734. https://doi.org/10.1016/j.molstruc.2024.139734

Oladipo, S. D., Luckay, R. C., Olalekan, S. O., Badeji, A. A., Matinise, N., & Tshikhudo, F. (2025b). Investigating the Inhibitory Potential of Halogenated Quinoline Derivatives against MAO-A and MAO-B: Synthesis, Crystal Structure,

Density Functional Theory, and Molecular Dynamics Simulations. ACS Omega, 10(25), 26500–26519. https://doi.org/10.1021/acsomega.4c11530

Oladipo, S. D., Luckay, R. C., Olalekan, S. O., Badeji, A. A., Yusuf, T. L., Adeleke, A. A., & Matinise, N. (2025c). Probing the Inhibitory Potential of Halogenated Symmetrical Formamidine Against MAO‐A and MAO‐B: Structural Elucidation, Molecular Dynamic Simulation and DFT Computational Studies. Chemistry & Biodiversity, e00886. https://doi.org/10.1002/cbdv.202500886

Olalekan, S. O., Bakare, O. O., Okwute, P. G., Osonuga, I. O., Adeyanju, M. M., & Olalekan, R. O. (2024a). The role of nutraceuticals in managing metabolic syndrome: A review of clinical studies. The Egyptian Journal of Internal Medicine, 36(1), 108. https://doi.org/10.1186/s43162-024-00375-9

Olalekan, S. O., Obakachi, V. A., Badeji, A. A., Akinsipo, O. B., Familoni, O., Asekun, O. T., Oladipo, S. D., & Osinubi, A. D. (2024b). Exploring the therapeutic potential of prolinamides as multi-targeted agents for Alzheimer's disease treatment: Molecular docking and molecular dynamic simulation studies. In Silico Pharmacology, 12(2), 80. https://doi.org/10.1007/s40203-024-00250-z

Olalekan, S. O., Okwute, P. G., Osonuga, I. O., & Adeyanju, M. M. (2024c). A review of botanical interventions for neuropathy and neuropathic pain. Clinical Phytoscience, 10(1), 23. https://doi.org/10.1186/s40816-024-00385-8

Ortix, C. (2021). Nonlinear Hall Effect with Time‐Reversal Symmetry: Theory and Material Realizations. Advanced Quantum Technologies, 4(9), 2100056. https://doi.org/10.1002/qute.202100056

Osonuga, I. O., Ogunlade, A. A., Olalekan, S. O., Okebule, B., & Olukade, B. A. (2020). The effect of aqueous leaves extract of Moringa Oleiferaon testosterone and prolactin level in adult male wistar rats (rattus norvegicus). Nigerian Journal of Scientific Research, 19(3), 175–180. https://scholar.google.com/scholar?cluster=12740782255403316786&hl=en&oi=scholarr

Pal, R., & Chattaraj, P. K. (2023). Electrophilicity index revisited. Journal of Computational Chemistry, 44(3), 278–297.

Parr, R. G., Donnelly, R. A., Levy, M., & Palke, W. E. (1978). Electronegativity: The density functional viewpoint. The Journal of Chemical Physics, 68(8), 3801–3807. https://doi.org/10.1063/1.436185

Paton, D.M. (2020). Istradefylline: Adenosine A2A receptor antagonist to reduce "OFF"time in Parkinson's disease. Drugs of Today, 56(2), 125. https://doi.org/10.1358/dot.2020.56.2.3098156

Pearson, R. G. (2005). Chemical hardness and density functional theory. Journal of Chemical Sciences, 117(5), 369–377. https://doi.org/10.1007/BF02708340

Rinaldi, D. (2025). Motor and non-motor symptoms in advanced Parkinson's disease: Current insights and future directions.

Saini, N., Singh, N., Kaur, N., Garg, S., Kaur, M., Kumar, A., Verma, M., Singh, K., & Sohal, H. S. (2024). Motor and non-motor symptoms, drugs, and their mode of action in Parkinson's disease (PD): A review. Medicinal Chemistry Research, 33(4), 580–599.

Salmaso, V., & Moro, S. (2018). Bridging Molecular Docking to Molecular Dynamics in Exploring Ligand-Protein Recognition Process: An Overview. Frontiers in Pharmacology, 9, 923. https://doi.org/10.3389/fphar.2018.00923

Salo-Ahen, O. M. H., Alanko, I., Bhadane, R., Bonvin, A. M. J. J., Honorato, R. V., Hossain, S., Juffer, A. H., Kabedev, A., Lahtela-Kakkonen, M., Larsen, A. S., Lescrinier, E., Marimuthu, P., Mirza, M. U., Mustafa, G., Nunes-Alves, A., Pantsar, T., Saadabadi, A., Singaravelu, K., & Vanmeert, M. (2020). Molecular Dynamics Simulations in Drug Discovery and Pharmaceutical Development. Processes, 9(1), 71. https://doi.org/10.3390/pr9010071

Saramowicz, K., Siwecka, N., Galita, G., Kucharska-Lusina, A., Rozpędek-Kamińska, W., & Majsterek, I. (2023). Alpha-synuclein contribution to neuronal and glial damage in Parkinson's disease. International Journal of Molecular Sciences, 25(1), 360.

Seifert, E. (2014). OriginPro 9.1: Scientific data analysis and graphing software—software review.

Sert, Y., Albayati, M. R., Şen, F., & Dege, N. (2024). The DFT and in-silico analysis of 2,2′-((1e,1′e)-((3,3′-dimethyl-[1,1′-biphenyl]−4,4′diyl)bis(azanylylidene))bis(methanylylidene))diphenol molecule. Colloids and Surfaces A: Physicochemical and Engineering Aspects, 687, 133444. https://doi.org/10.1016/j.colsurfa.2024.133444

Shelley, J. C., Cholleti, A., Frye, L. L., Greenwood, J. R., Timlin, M. R., & Uchimaya, M. (2007). Epik: A software program for pK a prediction and protonation state generation for drug-like molecules. Journal of Computer-Aided Molecular Design, 21(12), 681–691. https://doi.org/10.1007/s10822-007-9133-z

Sin, K.-R., Kim, C.-J., Ko, S.-G., Hwang, T.-M., Han, Y.-N., & Pak, Y.-N. (2022). Inclusion of thymol into cucurbiturils: Density functional theory approach with dispersion correction and natural bond orbital analysis. Journal of Inclusion Phenomena and Macrocyclic Chemistry, 102(5–6), 533–542. https://doi.org/10.1007/s10847-022-01135-4

Su, D., Cui, Y., He, C., Yin, P., Bai, R., Zhu, J., Lam, J. S., Zhang, J., Yan, R., & Zheng, X. (2025). Projections for prevalence of Parkinson's disease and its driving factors in 195 countries and territories to 2050: Modelling study of Global Burden of Disease Study 2021. Bmj, 388.

Suresh, C. H., Remya, G. S., & Anjalikrishna, P. K. (2022). Molecular electrostatic potential analysis: A powerful tool to interpret and predict chemical reactivity. WIREs Computational Molecular Science, 12(5), e1601. https://doi.org/10.1002/wcms.1601

Szewczuk, N. A., Duchowicz, P. R., Pomilio, A. B., & Lobayan, R. M. (2023). Resonance structure contributions, flexibility, and frontier molecular orbitals (HOMO–LUMO)

of pelargonidin, cyanidin, and delphinidin throughout the conformational space: Application to antioxidant and antimutagenic activities. Journal of Molecular Modeling, 29(1), 2. https://doi.org/10.1007/s00894-022-05392-5

Tan, Y.-Y., Jenner, P., & Chen, S.-D. (2022). Monoamine Oxidase-B Inhibitors for the Treatment of Parkinson's Disease: Past, Present, and Future. Journal of Parkinson's Disease, 12(2), 477–493. https://doi.org/10.3233/JPD-212976

Waggan, I., Rissanen, E., Tuisku, J., Joutsa, J., Helin, S., Parkkola, R., Rinne, J. O., & Airas, L. (2023). Adenosine A2A receptor availability in patients with early- and moderate-stage Parkinson's disease. Journal of Neurology, 270(1), 300–310. https://doi.org/10.1007/s00415-022-11342-1

Wang, J., Wolf, R. M., Caldwell, J. W., Kollman, P. A., & Case, D. A. (2004). Development and testing of a general amber force field. Journal of Computational Chemistry, 25(9), 1157–1174. https://doi.org/10.1002/jcc.20035

Weigend, F. (2006). Accurate Coulomb-fitting basis sets for H to Rn. Physical Chemistry Chemical Physics, 8(9), 1057. https://doi.org/10.1039/b515623h

Yang, K., Zheng, J., Zhao, Y., & Truhlar, D. G. (2010). Tests of the RPBE, revPBE, τ-HCTHhyb, ωB97X-D, and MOHLYP density functional approximations and 29 others against representative databases for diverse bond energies and barrier heights in catalysis. The Journal of Chemical Physics, 132(16), 164117. https://doi.org/10.1063/1.3382342

Yao, X.-Y., Guan, L.-N., Chen, Q., & Ren, C. (2024). LRRK2 G2019S and Parkinson's disease: Insight from Neuroinflammation. Postgraduate Medical Journal, 100(1179), 4–11. https://academic.oup.com/pmj/article-abstract/100/1179/4/7287096

Ylilauri, M., & Pentikäinen, O. T. (2013). MMGBSA As a Tool To Understand the Binding Affinities of Filamin–Peptide Interactions. Journal of Chemical Information and Modeling, 53(10), 2626–2633. https://doi.org/10.1021/ci4002475

Zhan, C.-G., Nichols, J. A., & Dixon, D. A. (2003). Ionization Potential, Electron Affinity, Electronegativity, Hardness, and Electron Excitation Energy: Molecular Properties from Density Functional Theory Orbital Energies. The Journal of Physical Chemistry A, 107(20), 4184–4195. https://doi.org/10.1021/jp0225774

Zhao, T., Li, C., Wang, S., & Song, X. (2022). Green tea (Camellia sinensis): A review of its phytochemistry, pharmacology, and toxicology. Molecules, 27(12), 3909. https://www.mdpi.com/1420-3049/27/12/3909

Zhao, Y., Zhou, Y.-G., & Chen, J.-F. (2024). Targeting the adenosine A2A receptor for neuroprotection and cognitive improvement in traumatic brain injury and Parkinson's disease. Chinese Journal of Traumatology, 27(3), 125–133. https://doi.org/10.1016/j.cjtee.2023.08.003

Zhu, H., Tonelli, F., Turk, M., Prescott, A., Alessi, D. R., & Sun, J. (2023). Rab29-dependent asymmetrical activation of leucine-rich repeat kinase 2. Science, 382(6677), 1404–1411. https://doi.org/10.1126/science.adi9926

Zhu, J., Cui, Y., Zhang, J., Yan, R., Su, D., Zhao, D., Wang, A., & Feng, T. (2024). Temporal trends in the prevalence of Parkinson's disease from 1980 to 2023: A systematic review and meta-analysis. The Lancet Healthy Longevity, 5(7), e464–e479.

APPENDIX

Table S1: Phytochemicals Present in *Camellia Sinensis*

S/N	Phytochemicals	PubChem CID
1	Catechin	9064
2	Epicatechin	72276
3	Epigallocatechin	72277
4	Epicatechin gallate	107905
5	Epigallocatechin_gallate	65064
6	Myricetin-3-galactoside	5491408
7	Myricetin 3-rhamnoside-7-glucoside	44259447
8	Myricetin-3-glucoside	5486615
9	Quercetin-3-rhamnosylglucoside	5491657
10	Quercetin-3-galactoside	5281643
11	Quercetin-3-glucoside	5280804
12	kaempferol-3-galactoside	5282149
13	Cyanidin	128861
14	Pelargonidin	440832
15	Malvidin	159287
16	Petunidin	441774
17	Gallic Acid	370
18	Chlorogenic Acid	1794427
19	Caffeic Acid	689043

S/N	Phytochemicals	PubChem CID
20	p-Coumaric acid	637542
21	Ellagic Acid	5281855
22	Quinic acid	6508
23	Caffeine	2519
24	Theophylline	2153
25	Theobromine	5429

Table S2: Binding Affinities of Reference Ligands and *Camellia Sinensis* Phytochemicals with Proteins of Interest

Phytochemical	PubChem CID	Protein Targets – Glide Score		
		LRRK2	A2AR	MAO-B
Reference Drugs				
DNL201 (LRRK2)	69093374	-5.92	-	-
Istradefylline (A2AR)	5311037	-	-8.82	-
Rasagiline (MAO-B)	3052776	-	-	-7.57
Phytochemicals in *Camellia sinensis*				
Epicatechin	72276	-8.14	-7.83	-8.58
Cyanidin	128861	-7.78	-7.69	-10.25
Pelargonidin	440832	-7.14	-8.23	-9.83
Petunidin	441774	-7.17	-7.49	-9.85
Malvidin	159287	-6.87	-7.12	-9.96
Epigallocatechin	72277	-5.52	-8.07	-8.54
Epigallocatechin Gallate	65064	-6.78	-6.85	-
Epicatechin Gallate	107905	-6.44	-6.28	-8.63
Caffeine	2519	-6.97	-7.52	-7.57
Theobromine	5429	-6.97	-7.52	-7.57
Theophylline	2153	-6.83	-7.77	-7.71
Catechin	9064	-	-7.80	-9.85
Ellagic Acid	5281855	-7.22	-7.74	-8.33
Myricetin-3-glucoside	5486615	-5.63	-7.73	-7.85
Myricetin 3-rhamnoside-7-glucoside	44259447	-4.20	-7.27	-
Quercetin-3-glucoside	5280804	-5.72	-5.61	-
Quercetin-3-galactoside	5281643	-4.72	-5.12	-
Quercetin-3-rhamnosylglucoside	5491657	-4.36	-2.86	-
Kaempferol-3-galactoside	5282149	-5.10	-4.85	-
Myricetin-3-galactoside	5491408	-5.06	-5.19	-
p-Coumaric Acid	637542	-6.04	-5.37	-6.04
Caffeic Acid	689043	-5.69	-5.86	-5.93
Gallic Acid	370	-5.95	-	-
Chlorogenic Acid	1794427	-5.49	-6.66	-8.36
Quinic Acid	6508	-5.53	-5.75	-7.16